

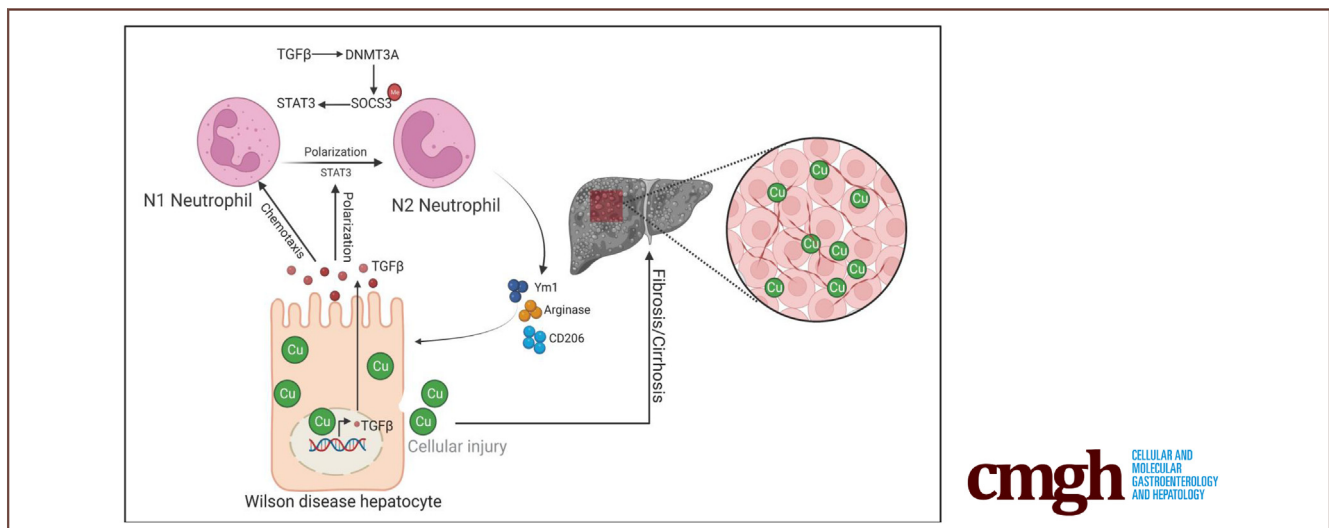
ORIGINAL RESEARCH

Stimulation of Liver Fibrosis by N2 Neutrophils in Wilson's Disease



Xiaoxiao Mi,¹ Yu Song,² Chaohua Deng,³ Jian Yan,¹ Zhihui Li,⁴ Yingniang Li,⁵ Jun Zheng,⁶ Wenjun Yang,⁶ Ling Gong,³ and Junping Shi^{1,3,7}

¹Institute of Translational Medicine, The Affiliated Hospital of Hangzhou Normal University, Hangzhou, Zhejiang, China; ²Department of Hepatology, The Second Affiliated Hospital of Zhejiang Chinese Medical University, Xinhua Hospital of Zhejiang Province, Hangzhou, Zhejiang, China; ³Department of Infectious Diseases and Hepatology, The Affiliated Hospital of Hangzhou Normal University, Hangzhou, Zhejiang, China; ⁴Clinical Research Center, The Second Affiliated Hospital, School of Medicine, Zhejiang University, Hangzhou, Zhejiang, China; ⁵School of Medicine, Zhejiang University, Hangzhou, Zhejiang, China; ⁶Department of Pathology, The Affiliated Hospital of Hangzhou Normal University, Hangzhou, Zhejiang, China; and ⁷Institute of Hepatology and Metabolic Diseases, Hangzhou Normal University, Zhejiang, China



SUMMARY

Transforming growth factor is highly expressed in hepatocytes and is associated with liver N2 neutrophil formation in Wilson's disease. Specific transforming growth factor inhibition or methylation inhibition modulates neutrophil function, attenuates parenchymal liver fibrosis, and reduces liver injury in Wilson's disease.

BACKGROUND & AIMS: Wilson's disease is an inherited hepatoneurologic disorder caused by mutations in the copper transporter ATP7B. Liver disease from Wilson's disease is one leading cause of cirrhosis in adolescents. Current copper chelators and zinc salt treatments improve hepatic presentations but frequently worsen neurologic symptoms. In this study, we showed the function and machinery of neutrophil heterogeneity using a zebrafish/murine/cellular model of Wilson's disease.

METHODS: We investigated the neutrophil response in *atp7b*^{-/-} zebrafish by live imaging, movement tracking, and transcriptional analysis in sorted cells. Experiments were conducted to

validate liver neutrophil heterogeneity in *Atp7b*^{-/-} mice. In vitro experiments were performed in ATP7B-knockout human hepatocellular carcinomas G2 cells and isolated bone marrow neutrophils to reveal the mechanism of neutrophil heterogeneity.

RESULTS: Recruitment of neutrophils into the liver is observed in *atp7b*^{-/-} zebrafish. Pharmacologic stimulation of neutrophils aggravates liver and behavior defects in *atp7b*^{-/-} zebrafish. Transcriptional analysis in sorted liver neutrophils from *atp7b*^{-/-} zebrafish reveals a distinct transcriptional profile characteristic of N2 neutrophils. Furthermore, liver N2 neutrophils also were observed in ATP7B-knockout mice, and pharmacologically targeted transforming growth factor β 1, DNA methyltransferase, or signal transducer and activator of transcription 3 reduces liver N2 neutrophils and improves liver function and alleviates liver inflammation and fibrosis in ATP7B-knockout mice. Epigenetic silencing of *Socs3* expression by transforming growth factor β 1 contributes to N2-neutrophil polarization in isolated bone marrow neutrophils.

CONCLUSIONS: Our findings provide a novel prospect that pharmacologic modulation of N2-neutrophil activity should

be explored as an alternative therapeutic to improve liver function in Wilson's disease. (*Cell Mol Gastroenterol Hepatol* 2023;16:657–684; <https://doi.org/10.1016/j.jcmgh.2023.06.012>)

Keywords: Wilson's Disease; Liver Fibrosis; Neutrophil Heterogeneity; N2 Neutrophils.

Wilson's disease (also called *progressive hepatolenticular degeneration*) is an autosomal-recessive inherited disease caused by pathogenic variants in the *ATP7B* gene, which is a copper transporting adenosine triphosphatase expressed mainly in hepatocytes.¹ Approximately 60% of index patients with Wilson's disease present with hepatic syndromes, and approximately 50%–60% of patients eventually develop liver cirrhosis.² Disorders of copper metabolism in Wilson's disease cause pathologic changes in the liver with fibrosis, which is an essential stage in the progression to cirrhosis.³ Copper accumulates in the liver and later in the brain, and, if untreated, it invariably will result in severe disability and death in patients. Drug interventions (such as copper chelators and zinc salts) reduce pathologic copper deposition, but side effects can be observed in up to 40% of patients during treatment and even after years of treatment, particularly nephropathy, autoimmune conditions, and skin changes.^{4,5} Liver transplantation is an effective treatment for Wilson's disease, particularly for patients with end-stage liver disease, but donor shortages and lifelong immunosuppression limit its use.⁶ Therefore, alternative treatments with higher specificity in Wilson's disease patients are urgently needed.

The existence of phenotypic heterogeneity and functional versatility of neutrophils in different environmental cues has been reported.^{7–9} Phenotypically heterogeneous and functionally versatile populations of neutrophils govern how they respond to environmental cues.⁷ Persistent neutrophil infiltration leads to chronic tissue inflammation and damage, and unresolved inflammation creates a microenvironment facilitating tumor formation. Dual roles and polarized phenotypes of neutrophils have been reported, denominated as N1 and N2.¹⁰ N1 neutrophils have proinflammatory/antitumor roles, are characterized by high expression of inflammatory factors, and show high levels of reduced nicotinamide adenine dinucleotide phosphate oxidase activity with consequent production of reactive oxygen species, which are cytotoxic to tumor cells; N2 neutrophils have anti-inflammatory/protumor activity, are characterized by high levels of arginase/CD206/Ym1, and have high proangiogenic and immunosuppressive activity.^{11–13} Nicotine-induced N2 neutrophils play a prometastatic role in breast cancer cell colonization in the lungs.¹⁴ Circulating N2 neutrophils also have been observed in noncancer inflammatory diseases such as systemic lupus erythematosus, myocardial infarction, and stroke.^{15–17} Patients with Wilson's disease, as a sterile inflammatory disease, have a risk of developing hepatocarcinogenesis. The annual risk of HCC in cirrhotic patients with Wilson's disease was estimated to be 0.14%,¹⁸ but liver malignancies occurred in another

cohort in 1.2% of patients, and the incidence was 0.28 per 1000 person years.¹⁹ Therefore, hepatocarcinogenesis in Wilson's disease may be more frequent than formerly appreciated. However, the heterogeneity of neutrophils in the pathogenesis and progression of Wilson's disease is poorly understood.


Herein, we addressed neutrophil heterogeneity in *Atp7b*^{-/-} mice and *atp7b*^{-/-} zebrafish, the latter of which is an earlier established invertebrate animal model for Wilson's disease.²⁰ We found the existence of N2 neutrophils during liver disease progression in *Atp7b*^{-/-} mice and *atp7b*^{-/-} fish. After pharmacologic ablation of N2 neutrophils, liver fibrosis was alleviated in *Atp7b*^{-/-} mice. Using isolated bone marrow neutrophils, we found that epigenetic silencing of *Socs3* expression by TGFβ1 contributed to N2-neutrophil polarization. Therefore, neutrophil heterogeneity shows therapeutic potential, and pharmacologic modulation of N2-neutrophil activity should be explored as an alternative therapeutic to improve liver function in Wilson's disease. Our results will contribute to the in-depth understanding of neutrophil biology and the development of treatments for Wilson's disease.

Results

Neutrophils Infiltrate the Liver and Accelerate Liver Defects in Wilson's Disease

To examine the neutrophil response in Wilson's disease, *atp7b*^{+/+} and *atp7b*^{-/-} zebrafish created earlier by our group²⁰ were crossed with *Tg(lyz:DsRED2)* fish for the production of offspring with *Dsred*-labeled neutrophils in vivo. We monitored *Dsred*-expressing neutrophils in the Cuprum (Cu) challenge window with a 6-hour interval in wild-type and mutant fish. As shown in Figure 1A, neutrophil infiltration was observed in mutant fish livers compared with wild-type fish livers. To quantify the liver-infiltrated neutrophils, neutrophil count and density (neutrophil number/liver area) were assessed. The liver neutrophil count and density were increased significantly in mutant fish compared with wild-type fish (Figure 1B–D).

Abbreviations used in this paper: ALT, alanine aminotransferase; AST, aspartate aminotransferase; ATP7B-KO, ATPase Copper Transporting Beta Polypeptide 7B-knockout; BSA, bovine serum albumin; cDNA, complementary DNA; Cu, Cuprum; DEG, differentially expressed gene; DNMT, DNA methyltransferase; FACS, fluorescence-activated cell sorting; FPRA14, Formyl peptide receptor agonist 14; HDL-C, high-density lipoprotein cholesterol; LPS, lipopolysaccharide; Ly6G, Lymphocyte antigen 6 family member G; mRNA, messenger RNA; NOS2, Nitric oxide synthase 2; PBS, phosphate-buffered saline; PR 39, Proline/arginine rich 39-amino-acid peptide; pSTAT3, Phosphorylated signal transducer and activator of transcription 3; qPCR, quantitative polymerase chain reaction; SM16, Small molecule ALK5/ALK4 kinase inhibitor; SOCS3, silence suppressor of cytokine signaling 3; STAT3, signal transducer and activator of transcription 3; STATTIC, Signal transducer and activator of transcription three inhibitory compound; TChol, Total cholesterol; TGFβ, transforming growth factor β; 5-aza, 5-Aza-2'-deoxycytidine.

 Most current article

© 2023 The Authors. Published by Elsevier Inc. on behalf of the AGA Institute. This is an open access article under the CC BY-NC-ND license (<http://creativecommons.org/licenses/by-nc-nd/4.0/>).

2352-345X

<https://doi.org/10.1016/j.jcmgh.2023.06.012>

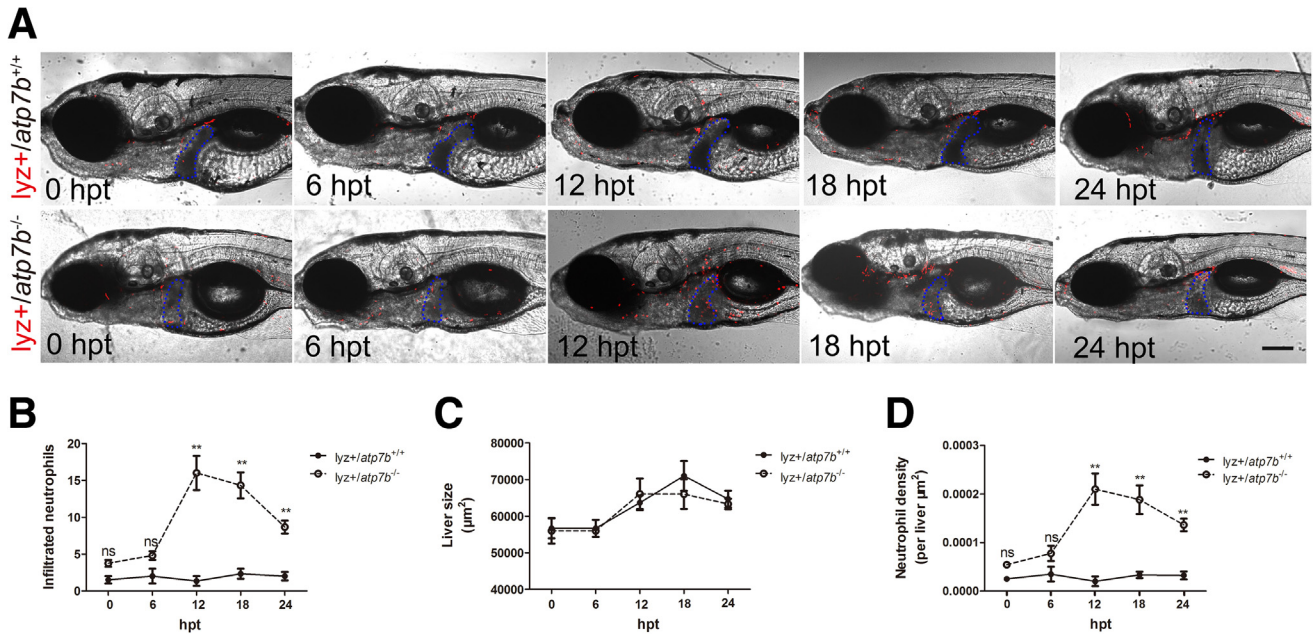


Figure 1. Neutrophils infiltrate into livers in *atp7b*^{-/-} zebrafish indicated by *lyz*-positive neutrophils. (A) Representative images of *lyz*^{+/+}/*atp7b*^{+/+} fish and *lyz*^{+/+}/*atp7b*^{-/-} fish after 0, 6, 12, 18, and 24 hours of Cu treatment. The livers are outlined in blue dashed lines. hpt, hours post-treatment. Scale bar: 200 µm. Liver (B) neutrophil count, (C) size, and (D) neutrophil density (liver neutrophil density = liver neutrophil count/liver size) in wild-type and mutant fish. Data are the means ± SEM, n = 10 fish/group. **P < .01.

These results revealed that neutrophils infiltrated into the liver during the pathogenesis of Wilson's disease. We also monitored neutrophils in *atp7b*^{+/+} and *atp7b*^{-/-} offspring with an *EGFP*⁺ background by crossing the wild-type and mutant fish with *Tg(mpx:EGFP)* fish, another fish expressing EGFP in neutrophils in vivo. As shown in Figure 2A and quantified in Figure 2B–D, significantly more liver-infiltrated neutrophils also were observed in mutant fish.

Collectively, we observed that neutrophils infiltrated the liver during the pathogenesis of Wilson's disease.

To examine the functional contribution of the infiltrated neutrophils, we assessed the effect of a general inflammatory stimulator, lipopolysaccharide (LPS), which has been shown to increase the infiltration of neutrophils under stress in zebrafish.²¹ In the presence of LPS, significant increases in liver neutrophil count and density were observed

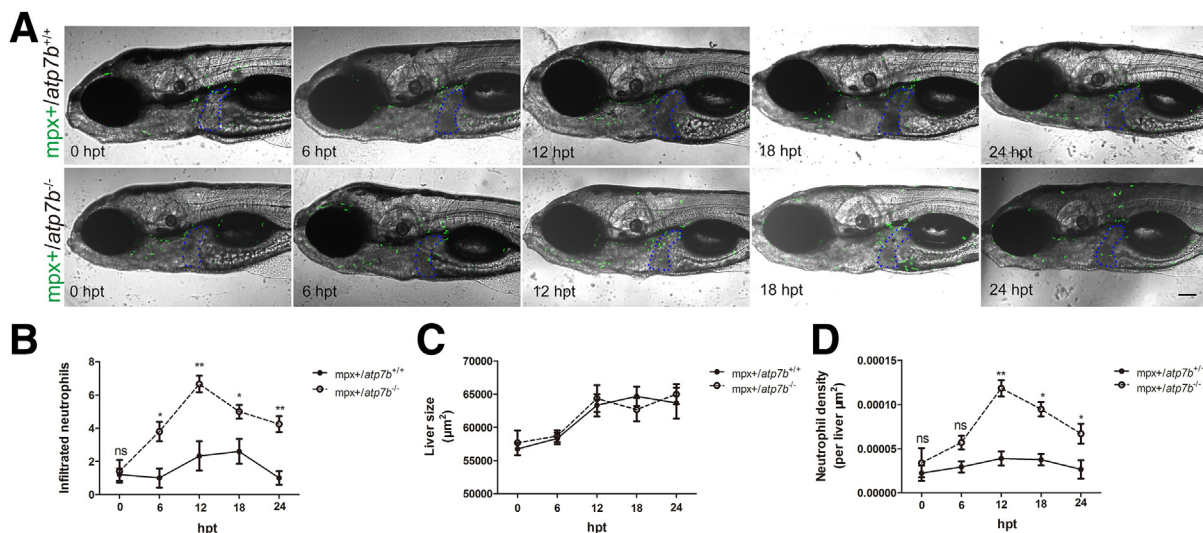


Figure 2. Neutrophils infiltrate into livers in *atp7b*^{-/-} zebrafish indicated by *mpx*-positive neutrophils. (A) Representative images of *mpx*^{+/+}/*atp7b*^{+/+} and *mpx*^{+/+}/*atp7b*^{-/-} fish after 0, 6, 12, 18, and 24 hours of Cu treatment. The livers are outlined in blue dashed lines. hpt, hours post-treatment. Scale bar: 200 µm. (B) Neutrophil count, (C) liver size, and (D) neutrophil density in wild-type and mutant fish livers. Data are the means ± SEM, n = 10 fish/group. *P < .05, **P < .01.

in both mutant and wild-type fish compared with the groups exposed to Cu alone (Figure 3). Histologically, in the presence of LPS, wild-type and mutant fish livers showed more lipid droplets and a more disorganized structure than the Cu-challenged group (Figure 4A). Another neutrophil-specific agonist, Formyl peptide receptor agonist 14 (FPR A14), also was used to challenge both mutant and wild-type fish under Cu exposure. Mutant fish livers, but not wild-type fish livers, exposed to FPR A14 had significantly more infiltrated neutrophils than that of the Cu alone group, as indicated by the neutrophil count and density (Figure 3). Moreover, under Cu plus FPR A14 challenge, mutant fish livers, but not wild-type fish livers, presented an increase in lipid droplets and a disorganized structure when compared with the group exposed to Cu alone (Figure 4A). To further dissect the role of neutrophils, mutant and wild-type fish were exposed to a neutrophil inhibitor, Proline/arginine rich 39-amino-acid peptide (PR 39), which has been shown to inhibit nicotinamide adenine dinucleotide phosphate oxidase activity in neutrophils.²² As shown in Figure 3, significant reduction of infiltrated liver neutrophil count and density were observed in mutant fish in the presence of PR 39, with a declining trend of infiltrated neutrophils in the

liver in wild-type fish. Histologically, mutant fish livers exposed to Cu and PR 39 treatment showed a reduction in lipid droplets and an ordered structure when compared with the group exposed to Cu alone (Figure 4A). We also assessed the expression of genes involved in lipid metabolism and neutrophils in the liver. In mutant fish, the expression of the lipid synthesis markers *ppar α* , *ppar γ* , *srebp1*, and *ucp2* was increased significantly in the Cu plus LPS- or Cu plus FPR A14-challenged group compared with the group exposed to Cu alone (Figure 4B-E). The expression of these lipid synthesis genes was reduced significantly in the Cu plus PR 39-treated group compared with the group exposed to Cu alone (Figure 4B-E). The expression of the neutrophil-specific factors *lyz* and *mpx* also was increased significantly in the Cu plus LPS- or Cu plus FPR A14-challenged mutant group compared with the mutant group exposed to Cu alone, and was reduced significantly in the Cu plus PR 39-treated mutant group compared with the mutant group exposed to Cu alone (Figure 4F and G). Furthermore, accumulated Cu in the mutant livers was increased significantly in the Cu plus LPS- or Cu plus FPR A14-challenged group and was not significantly changed in the Cu plus PR 39-treated group compared with the mutant

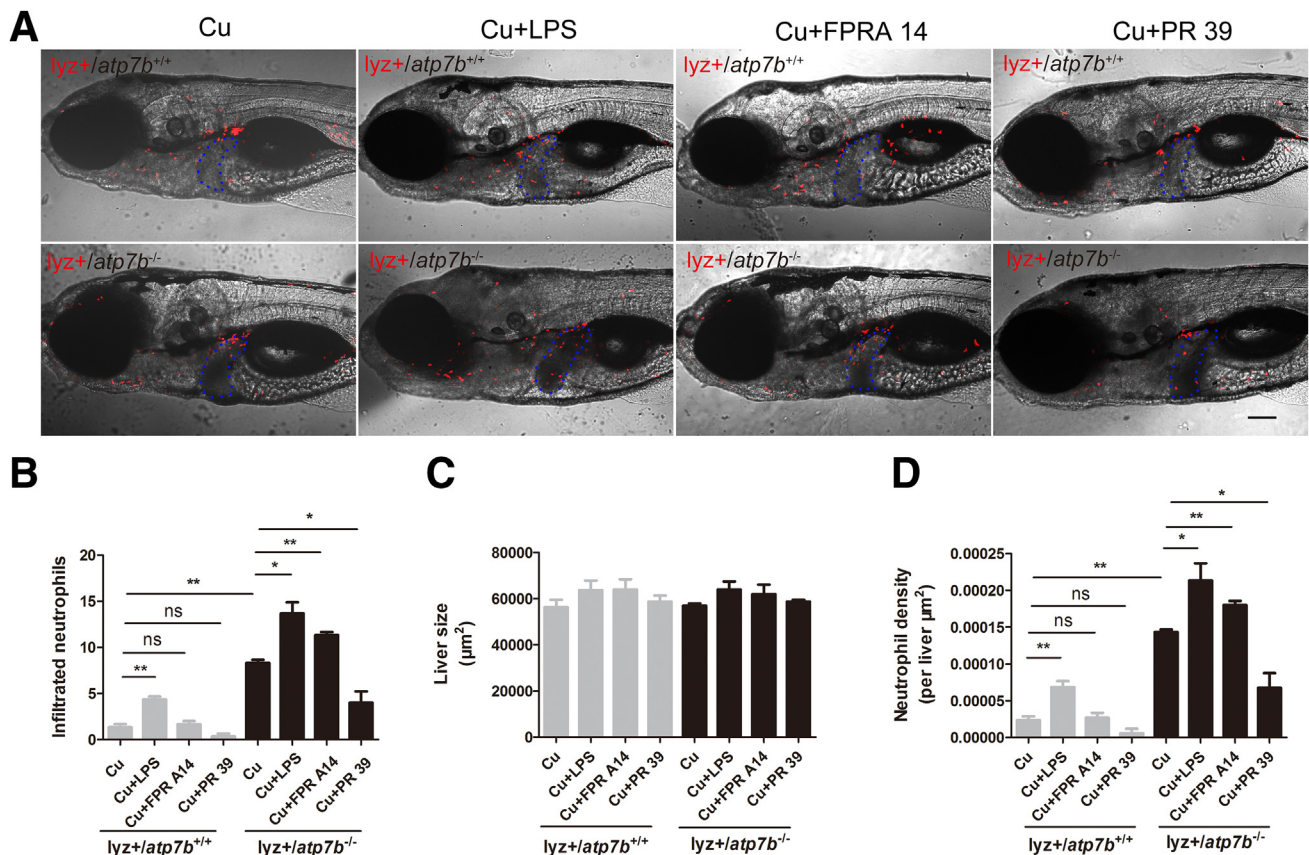


Figure 3. Effect of neutrophil activity-specific chemicals on liver-infiltrated neutrophils in *atp7b^{-/-}* zebrafish. (A) Representative images of *lyz+/atp7b^{+/+}* and *lyz+/atp7b^{-/-}* fish response to LPS, FPR A14, or PR 39 treatment. The livers are outlined in blue dashed lines. Scale bar: 200 μ m. (B) Neutrophil count, (C) liver size, and (D) neutrophil density in wild-type and mutant fish livers response to LPS, FPR A14, or PR 39 treatment. Data are the means \pm SEM, n = 10 fish/group. * $P < .05$, ** $P < .01$.

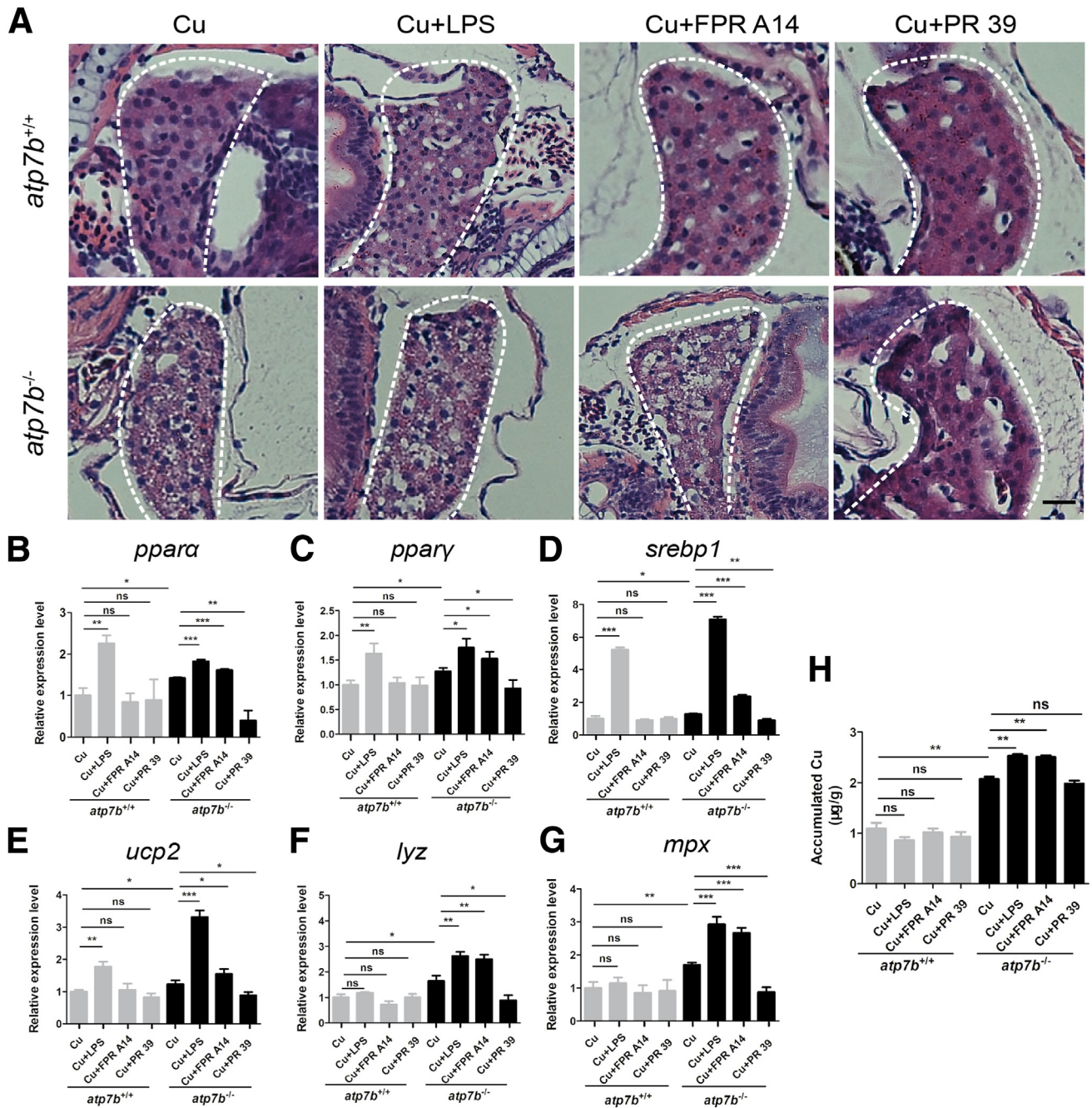


Figure 4. Effect of neutrophil activity-specific chemicals on liver pathogenesis in *atp7b*^{-/-} zebrafish. (A) Representative H&E staining images of liver sections from wild-type and mutant fish in response to LPS, FPR A14, or PR 39. Scale bar: 200 μm. qPCR of gene expression changes in the lipogenic factors (B) *pparα*, (C) *pparγ*, (D) *srebp1*, and (E) *ucp2*, and neutrophil-specific factors (F) *lyz* and (G) *mpx* in both wild-type and mutant fish livers response to LPS, FPR A14, or PR 39. Data are the means ± SEM, n = 3 sets of 20 fish/group. **P* < .05, ***P* < .01, ****P* < .001. (H) Inductively coupled plasma mass spectrometry of liver Cu content in wild-type and mutant fish in response to LPS, FPR A14, or PR 39. Data represent the means ± SEM, n = 3 sets of 1000 fish/group. ***P* < .01.

fish exposed to Cu alone (Figure 4H). We also measured the movement of wild-type and mutant fish under different pharmacologic challenges. As shown in Figure 5, the distance and velocity of the mutant fish were reduced significantly in the Cu plus LPS- or Cu plus FPR A14-challenged group compared with the Cu alone-exposed mutant group.

The mutant fish exposed to Cu plus PR 39 showed a slight but not significant increase in movement distance and velocity when compared with the group exposed to Cu alone. Collectively, these data suggested that neutrophils infiltrated the liver and accelerated liver defects in Wilson's disease.

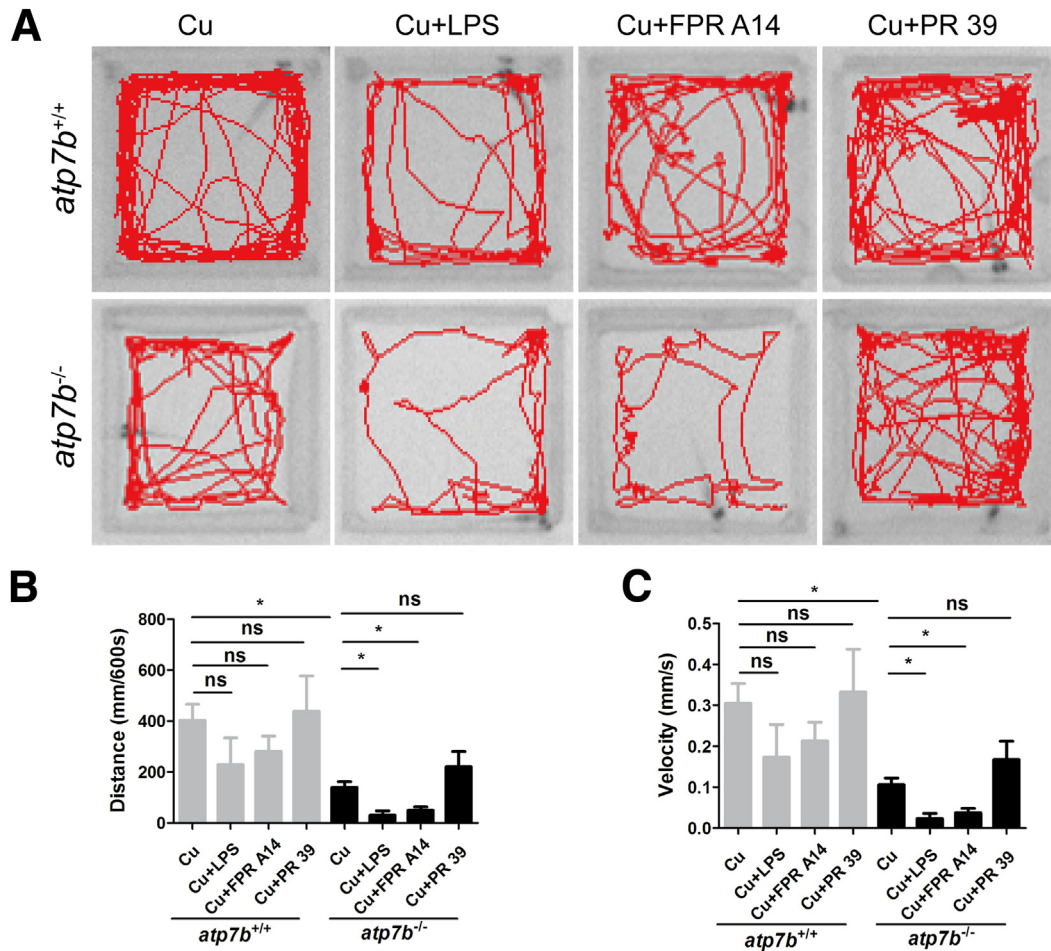


Figure 5. Effect of neutrophil activity-specific chemicals on movement deficits in *atp7b*^{-/-} zebrafish. (A) Representative images of ANY-maze (Noldus) analysis of swimming patterns in both wild-type and mutant fish response to LPS, FPR A14, or PR 39 treatment. Swimming (B) distance and (C) velocity in both wild-type and mutant fish response to LPS, FPR A14, or PR 39 treatment. Data are the means \pm SEM, $n = 3 \sim 4$ fish/group. * $P < .05$.

Liver-Infiltrated Neutrophils Display a Distinct Gene Transcriptional Profile in Wilson's Disease

To determine the gene transcriptional characteristics of liver-infiltrated neutrophils in Wilson's disease, we sorted liver neutrophils from mutant and wild-type fish and performed RNA sequencing assays. Based on a P value less than .05 and $|\log_2(\text{fold change})|$ greater than 1, we compared the differentially expressed genes (DEGs) between wild-type and mutant fish upon or without Cu challenge. The Venn diagram in Figure 6A showed that mostly DEGs were detected in the context of Cu challenge in the comparison of neutrophils from mutant fish vs wild-type fish. The volcano plot showed 561 up-regulated genes and 1417 down-regulated genes among DEGs in the comparison between the 2 groups (Figure 6B). Kyoto Encyclopedia of Genes and Genomes pathway enrichment analysis showed that the most significantly altered biological processes between the 2 groups were metabolism, including carbon metabolism, Peroxisome proliferator activated receptor (PPAR) signaling pathway, glycolysis/gluconeogenesis, biosynthesis of amino acids, glycine/serine/threonine metabolism, starch and

sucrose metabolism, glyoxylate and dicarboxylate metabolism, and phenylalanine metabolism (Figure 6C). The results suggested that metabolic adaptations have been identified in Wilson's disease liver neutrophils. It has been proposed that metabolic reprogramming is crucial for neutrophil differentiation and function.²³ We further analyzed the cytokine and chemokine expression profiles between the 2 groups. The heatmap showed a distinct cytokine and chemokine expression pattern of neutrophils in fish with Wilson's disease (Figure 6D). Quantitative polymerase chain reaction (qPCR) of selected genes validated the down-regulation of the most significantly changed cytokines and chemokines in Wilson's disease fish liver neutrophils compared with wild-type fish liver neutrophils (Figure 7A-H). Protein-Protein Interaction Networks analysis of the significantly changed cytokines and chemokines showed that the transforming growth factor β (TGF β) signaling pathway was in the central node among the significantly changed cytokines and chemokines (Figure 6E). Immunofluorescence analysis revealed that TGF β 1 was increased in *atp7b*^{-/-} fish liver compared with wild-type fish

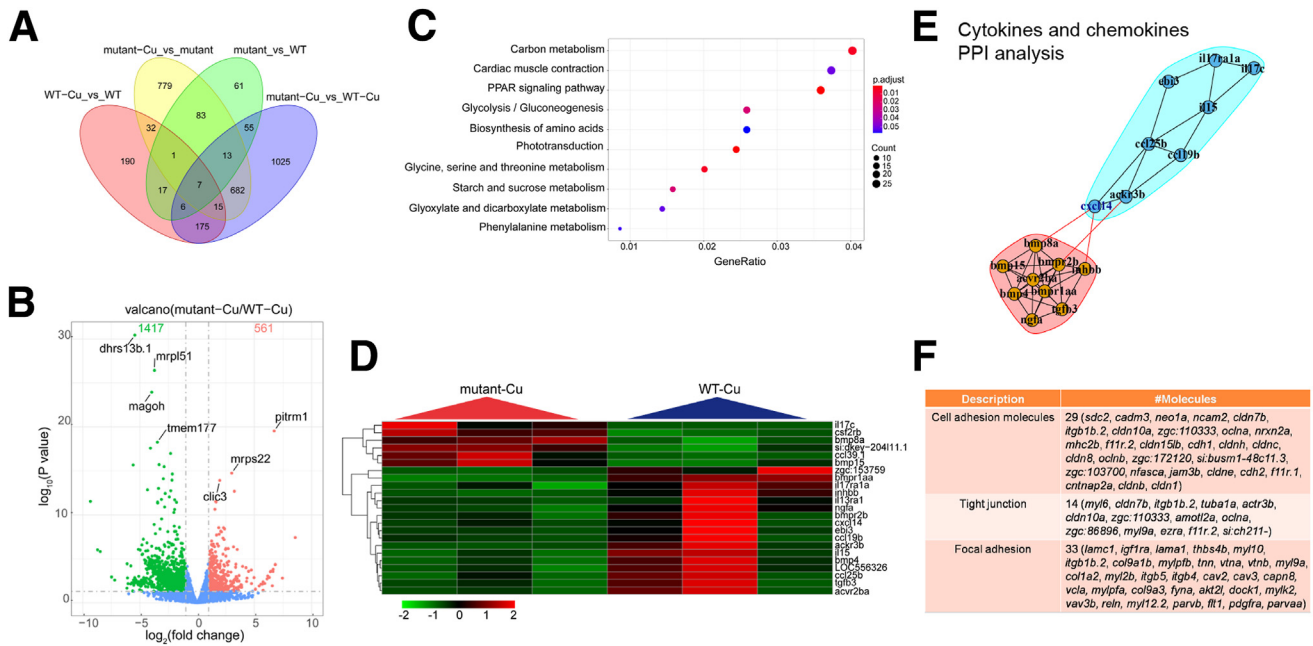


Figure 6. Gene transcriptional expression characteristics in *atp7b*^{-/-} zebrafish liver neutrophils. Liver neutrophils were sorted from wild-type and mutant fish, and transcriptome analysis was performed. (A) Venn diagram showed that the most DEGs were detected in the comparison between Cu-treated wild-type groups and Cu-treated mutant groups. (B) Volcano plot showed 561 up-regulated genes and 1417 down-regulated genes among DEGs were detected from comparison between Cu-treated wild-type groups and Cu-treated mutant groups. (C) Kyoto Encyclopedia of Genes and Genomes pathway enrichment analysis of the DEGs from comparison between Cu-treated wild-type groups and Cu-treated mutant groups. (D) Heatmap of the significantly changed cytokines and chemokines from comparison between Cu-treated wild-type groups and Cu-treated mutant groups. (E) Protein-Protein Interaction Networks analysis of the significantly changed cytokines and chemokines. (F) Ingenuity Pathway Analysis of cell adhesion, tight junction, and focal adhesion in Cu-treated wild-type groups and Cu-treated mutant groups. WT, wild-type.

liver in the context of Cu treatment (Figure 7I and J). In addition, the DEGs included 29 cell adhesion molecules, 14 tight junction molecules, and 33 focal adhesion molecules (Figure 6F). Collectively, these results revealed that liver-infiltrated neutrophils in Wilson's disease fish showed a distinct transcriptional profile and acquired an alternatively activated phenotype that is essential for liver disease progression.

Liver Infiltrated Neutrophils Polarize to the N2 Phenotype in Wilson's Disease

To further examine the functional properties of liver-infiltrated neutrophils, we assessed the polarization of liver neutrophils in an ATPase Copper Transporting Beta Polypeptide 7B-knockout (ATP7B-KO) mouse model (*Atp7b*^{-/-} mice) using N1-/N2-associated markers in mice. First, we monitored the physiopathology of ATP7B-KO mice at different ages. Specifically, the body weight of ATP7B-KO mice was reduced from 8 weeks of age compared with that of their wild-type littermates (Figure 8A). However, increased liver body ratio, alanine transaminase (ALT) level, and aspartate aminotransferase (AST) level were detected in 16-week-old and 24-week-old ATP7B-KO mice compared with the wild-type control (Figure 8B-D). Compared with wild-type mice, increased serum triglycerides were observed in 6-week-old and 8-week-old ATP7B-KO mice,

while decreased serum triglycerides were detected in 16-week-old and 24-week-old ATP7B-KO mice (Figure 8E). Reduced serum total cholesterol levels were observed in ATP7B-KO mice at all the measured time points compared with wild-type mice (Figure 8F). Low-density lipoprotein cholesterol was increased only in 8-week-old ATP7B-KO mice (Figure 8G). High-density lipoprotein cholesterol (HDL-C) was reduced at all the measured time points in ATP7B-KO mice (Figure 8H). H&E staining of liver sections showed widespread inflammation and necrosis in ATP7B-KO mice from 16 weeks of age until 24 weeks of age (Figure 8I). Furthermore, we isolated liver-infiltrated neutrophils and performed flow cytometry analysis. We found that liver-infiltrated neutrophils (CD11b+Lymphocyte antigen 6 family member G[Ly6G+]) were increased in ATP7B-KO mice at all the measured time points when compared with the wild-type control (Figure 9A and B). Among total liver-infiltrated neutrophils, more N2-type neutrophils (CD206+) than N1-type neutrophils (Nitric oxide synthase 2 [NOS2+]) were detected in ATP7B-KO mice from 8 weeks of age until 24 weeks of age (Figure 9A and C). In addition, the migratory pattern of neutrophils was tracked using confocal time-lapse imaging in *atp7b*^{+/+} fish and *atp7b*^{-/-} fish on a *lyz*⁺ background. The differences in neutrophil movement between wild-type and mutant fish were illustrated using Imaris software. As shown in Figure 9D, in approximately 2-hour

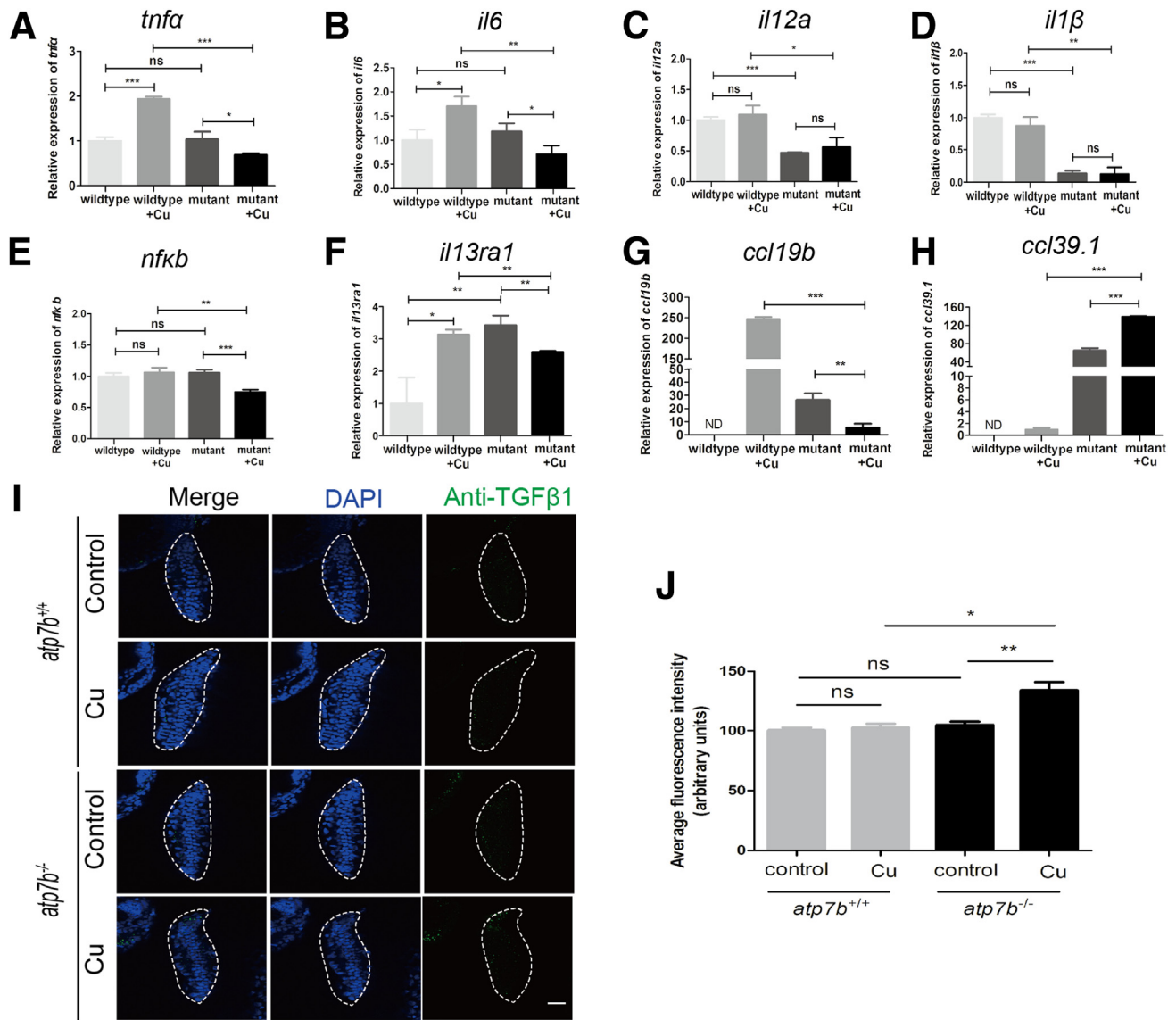


Figure 7. Experimental confirmation of the gene transcriptional profiles in *atp7b*^{-/-} zebrafish neutrophils. qPCR of the selected significantly changed cytokines and chemokines including (A) *tnfa*, (B) *il6*, (C) *il12a*, (D) *il1β*, (E) *nfkβ*, (F) *il13ra1*, (G) *ccl19b*, and (H) *ccl39.1* in sorted neutrophils from wild-type and mutant fish with/without Cu challenge. (I and J) Immunofluorescence staining of anti-TGFβ1 in wild-type and mutant fish with/without Cu challenge. Representative images of (I) immunofluorescence staining using anti-TGFβ1, and (J) average fluorescence intensity was quantified. The livers are outlined by white dashed lines. 4',6-Diamidino-2-phenylindole (DAPI) stains cell nuclei. Scale bar: 10 μm. (A–H and J) Data represent the means ± SEM. (A–H) n = 3 sets of neutrophils pooled from 600 larvae. (J) n = 10 fish/group. *P < .05, **P < .01, and ***P < .001.

time-lapse videos, within the liver, more infiltrated neutrophils with active movement were observed in mutant fish than in wild-type fish. We also performed Giemsa staining in isolated liver-infiltrated neutrophils in wild-type and mutant fish to examine the nuclear morphology. The results showed that more ring-formed nuclei than segmented nuclei were observed in mutant fish liver neutrophils than in wild-type fish liver neutrophils (Figure 9E). Collectively, these results suggested that liver-infiltrated neutrophils polarized to the N2 phenotype to play a crucial role in liver disease progression and cirrhosis development in Wilson's disease.

Pharmacologic Inhibition of N2 Neutrophils Improves Hepatic Presentations in Wilson's Disease

Since signal transducer and activator of transcription 3 (STAT3) is a critical transcription factor for N2-neutrophil polarization,¹⁴ we applied Signal transducer and activator of transcription three inhibitory compound (STAT3IC), a known STAT3 inhibitor, to wild-type and ATP7B-KO mice to test the effect of N2 neutrophils on hepatic pathogenesis. We observed that STAT3IC treatment increased the liver-infiltrated neutrophils both in wild-type and ATP7B-KO mice, but down-regulated the polarization of N2

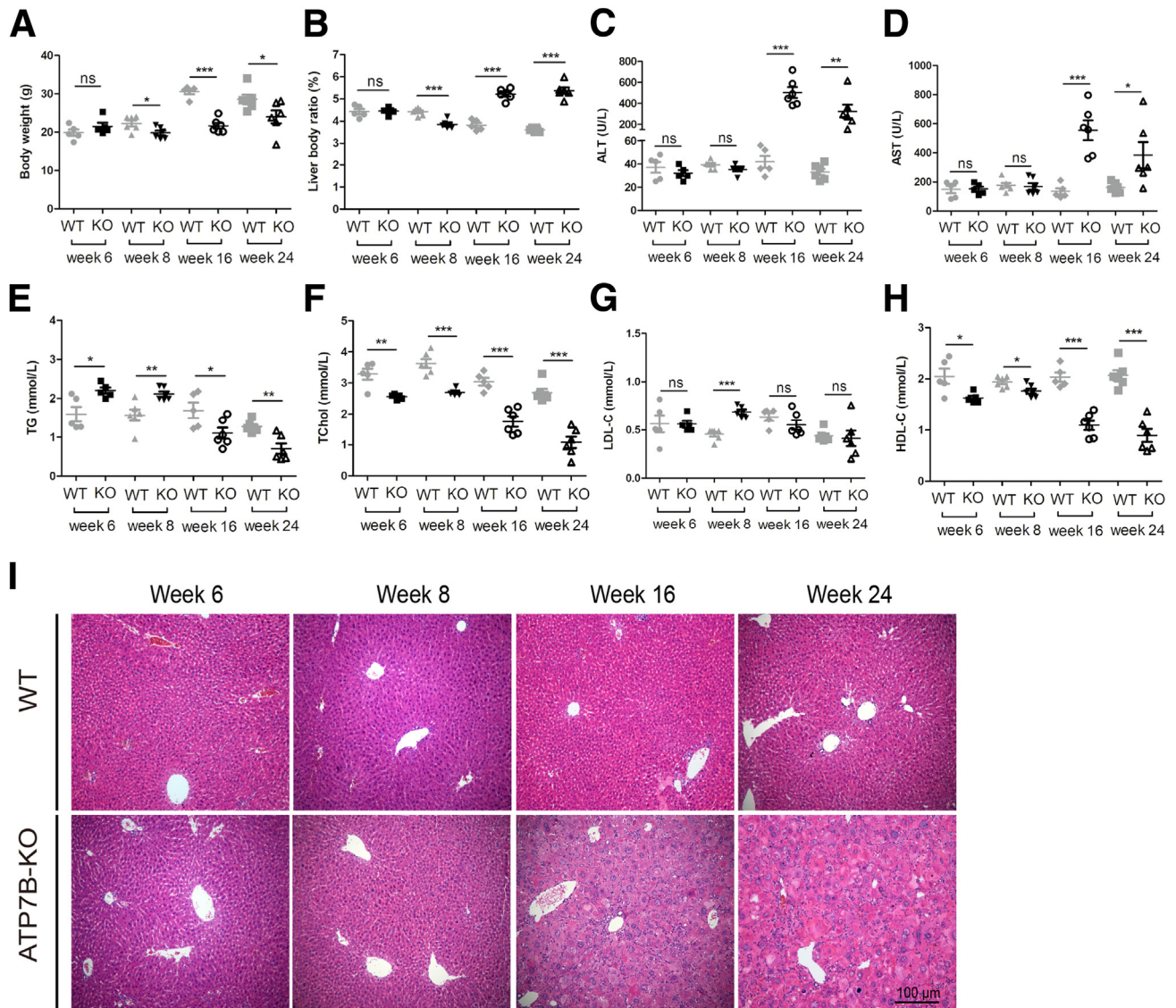
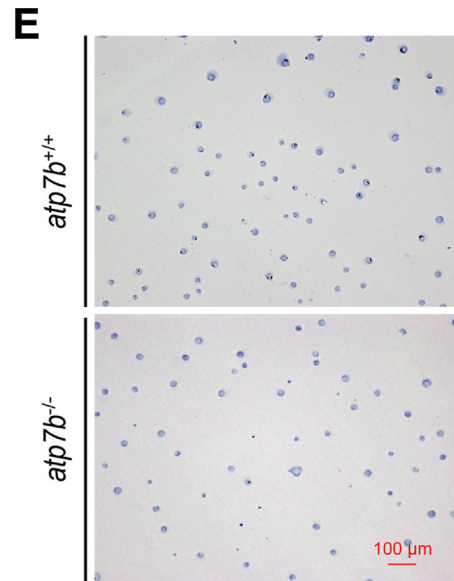
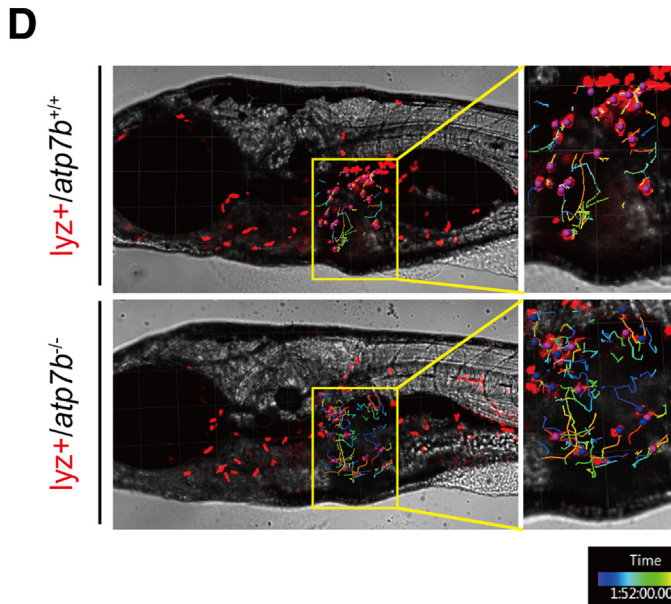
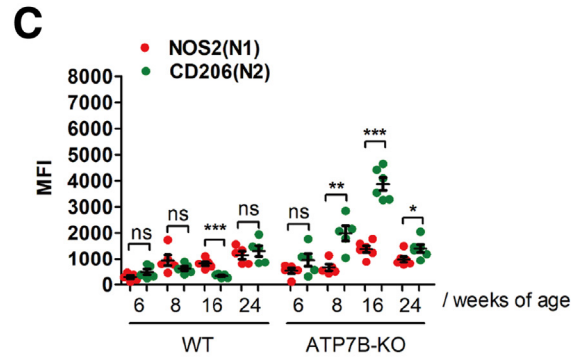
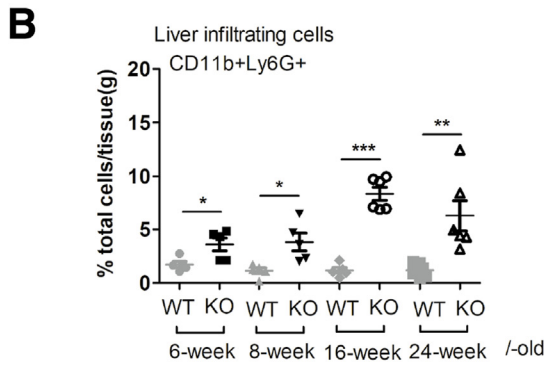
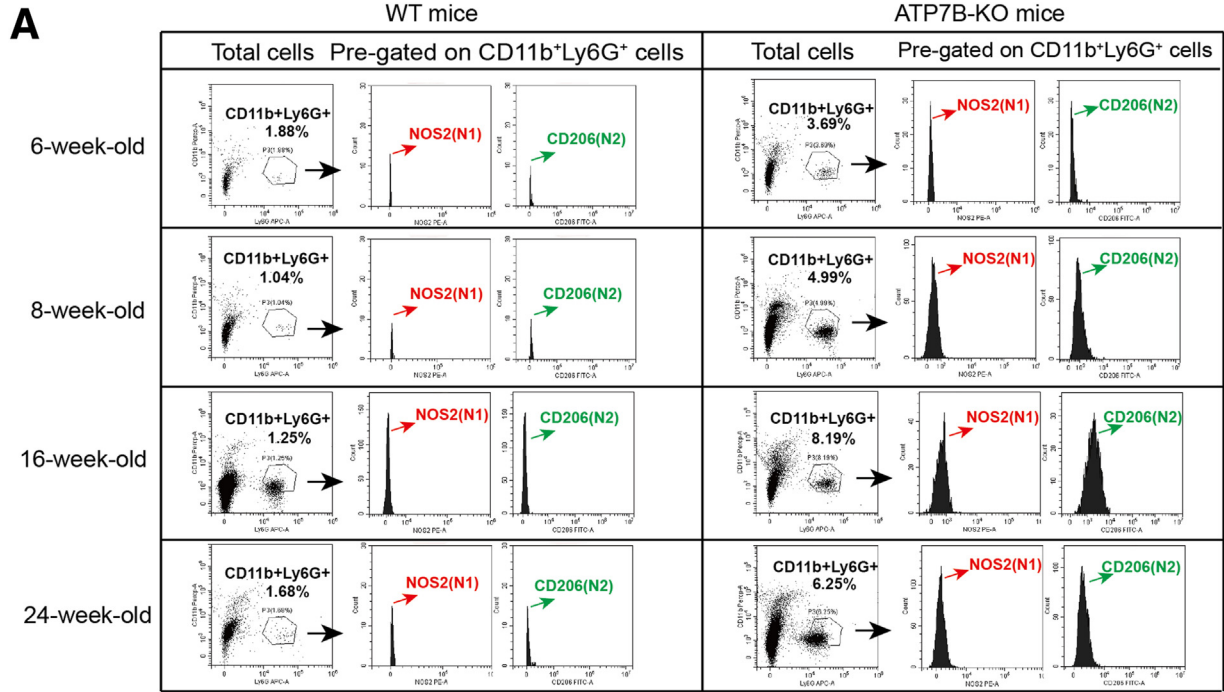


Figure 8. The development of liver defects in ATP7B-KO mice. (A) Body weight in 6-, 8-, 16-, and 24-week-old wild-type and ATP7B-KO mice. $n = 5 \sim 6$ mice/group. $*P < .05$, $***P < .001$. (B) Liver body ratio in 6-, 8-, 16-, and 24-week-old wild-type and ATP7B-KO mice. $n = 5 \sim 6$ mice/group. $***P < .001$. Serum activities of (C) ALT, (D) AST, (E) Triglyceride, (F) TChol, (G) low-density lipoprotein cholesterol (LDL-C), and (H) HDL-C in 6-, 8-, 16-, and 24-week-old wild-type and ATP7B-KO mice. $n = 5 \sim 6$ mice/group. $*P < .05$, $**P < .01$, and $***P < .001$. (I) Representative H&E images in liver sections from 6-, 8-, 16-, and 24-week-old wild-type and ATP7B-KO mice. Scale bar: 100 μm . WT, wild-type.

neutrophils only in ATP7B-KO mice (Figure 10A–C). Biochemical parameters, such as ALT, AST, HDL-C, and Total cholesterol (TChol), also were improved upon STAT3C treatment in ATP7B-KO mice, but not in wild-type mice (Figure 10D–G). We also observed a decreased liver body ratio upon STAT3C treatment in ATP7B-KO mice, which was comparable with the levels in wild-type mice with or without STAT3C treatment (Figure 10H). However, liver copper levels were not changed significantly upon STAT3C treatment in ATP7B-KO mice and wild-type mice (Figure 10I). Moreover, pathologic phenotypes in ATP7B-KO mouse livers with karyomegaly, cytomegaly, binucleate hepatocytes, intranuclear vacuoles, and necrosis also were alleviated upon STAT3C treatment (Figure 10J). Thus, these

results suggested that inhibition of N2-neutrophil polarization through pharmacologic targeting of STAT3 alleviated hepatic damage in Wilson's disease.

Furthermore, we adopted a neutrophil elastase inhibitor to treat wild-type and ATP7B-KO mice to increase liver N2 neutrophils *in vivo* to determine the effects on hepatic pathogenesis. Because neutrophil elastase attenuates tumor growth and induces a CD8⁺ T-cell response,²⁴ and depletion of N2-polarized Tumor associated neutrophils (TANs) also inhibits tumor growth and allows for increased activity of CD8 cytotoxic T lymphocytes,⁷ we inferred that inhibition of neutrophil elastase may increase N2 neutrophils *in vivo*. We applied GW311616A,²⁵ an orally administered active neutrophil elastase inhibitor, to wild-type and ATP7B-KO



mice to test the effect of N2 neutrophils on hepatic pathology. We observed that GW311616A treatment increased the infiltrated neutrophils both in wild-type and in ATP7B-KO mice and increased the polarization of N2 neutrophils in both mice (Figure 11A–C). Biochemical parameters, such as ALT, AST, HDL-C, and TChol, were not changed significantly upon GW311616A treatment in ATP7B-KO mice, with more aggravated levels than those in wild-type mice (Figure 11D–G). We also observed a decreased liver body ratio upon GW311616A treatment in ATP7B-KO mice, but the ratio still was higher than that in wild-type mice with or without GW311616A treatment (Figure 11H). Liver copper levels were not changed significantly in ATP7B-KO mice upon GW311616A treatment and were still higher than the levels in wild-type mice with or without GW311616A treatment (Figure 11I). Moreover, pathologic phenotypes in ATP7B-KO mouse livers with karyomegaly, cytomegaly, binucleate hepatocytes, intranuclear vacuoles, and necrosis also were aggravated upon GW311616A treatment (Figure 11J). In addition, the earlier-described findings were validated in genetic neutrophil elastase-deficient mice (Figure 12). Thus, these data suggested that an increase in N2-neutrophil polarization aggravated hepatic damage in Wilson's disease.

TGFβ1–DNA Methyltransferase 3A–Suppressor of Cytokine Signaling 3–STAT3 Signaling Axis Promotes N2-Neutrophil Polarization in Wilson's Disease

TGFβ1 within the tumor microenvironment induces N2-neutrophil polarization.⁷ STAT3 is an essential transcription factor for N2-neutrophil polarization.¹⁴ In systemic sclerosis disease, TGFβ1 induces the expression of DNA methyltransferase in fibroblasts to silence the expression of *Socs3*, facilitating activation of *Stat3* to promote fibrogenesis.²⁶ We observed an increased level of TGFβ1 in ATP7B-KO mouse livers (Figure 13A). In isolated liver neutrophils, increased expression of *Dnmt3a* and *Stat3* with reduced expression of *Socs3* was observed in ATP7B-KO mice (Figure 13B). We inferred that TGFβ1 drives neutrophil polarization by DNA methylation to silence the expression of *Socs3* and thus facilitate the activation of STAT3. To evaluate our hypothesis, pharmacologic inhibition of the activity of TGFβ1 signaling or DNA methyltransferases (DNMTs) using Small molecule ALK5/ALK4 kinase inhibitor (SM16) or 5-Aza-2'-deoxycytidine (5-aza) was performed in wild-type and ATP7B-KO mice. We observed that SM16 or 5-aza did not influence liver-infiltrated neutrophils in wild-type mice, but

resulted in a decrease in liver-infiltrated neutrophils in ATP7B-KO mice (Figure 13C and D). In ATP7B-KO mice, SM16 decreased liver N2 neutrophils and increased liver N1 neutrophils. In wild-type mice, SM16 increased liver N1 neutrophils but did not decrease liver N2 neutrophils (Figure 13C and E). Decreased liver N2 neutrophils and increased liver N1 neutrophils also were observed in 5-aza-treated ATP7B-KO mice; neither liver N2 neutrophils nor N1 neutrophils were changed significantly in 5-aza-treated wild-type mice compared with the vehicle-treated control (Figure 13C–E). Biochemical parameters, such as ALT, AST, HDL-C, and TChol, also were improved upon SM16 or 5-aza treatment in ATP7B-KO mice, but not in wild-type mice (Figure 13F–J). We also observed a decreased liver body ratio upon SM16 or 5-aza treatment in ATP7B-KO mice, which was comparable with the levels in wild-type mice with or without SM16 or 5-aza treatment (Figure 13J). However, liver copper levels were not changed significantly upon SM16 or 5-aza treatment in ATP7B-KO mice and in wild-type mice (Figure 13K). Moreover, pathologic phenotypes in ATP7B-KO mouse livers with karyomegaly, cytomegaly, binucleate hepatocytes, intranuclear vacuoles, and necrosis also were alleviated upon SM16 or 5-aza treatment (Figure 13L). Furthermore, Sirius red staining showed that liver fibrosis was reduced in ATP7B-KO mice upon SM16, 5-aza, or STAT3C treatment, and increased in ATP7B-KO mice upon GW311616A treatment (Figure 14A). qPCR results showed that the expression of hepatic stellate cell activation markers, including *Tgfb1*, *Col1a1*, *Col1a2*, and *vimentin*, was reduced in ATP7B-KO mice upon STAT3C treatment and increased upon GW311616A treatment in ATP7B-KO mice (Figure 14B–E). In addition, the extent of liver fibrosis was increased from 16 weeks of age to 24 weeks of age in ATP7B-KO mice, but not in wild-type mice (Figure 14F). Macroscopic regeneration nodes of different sizes in the liver, indicating cirrhosis, were observed at 24 weeks of age in ATP7B-KO mice (Figure 14F). Considering the nearly same extent of down-regulation of liver N2-neutrophil polarization and alleviation of hepatic damage after STAT3C, SM16, or 5-aza treatment in Wilson's disease mice, it is reasonable that TGFβ1 drives neutrophil polarization by DNA methylation to facilitate the activation of STAT3.

To reveal the molecular mechanism of neutrophil polarization, we treated freshly isolated neutrophils from mouse bone marrow with recombinant TGFβ1 with/without 5-aza or STAT3C to assess the expression of N1/N2-associated markers and the expression changes of STAT3, DNMT3A, and SCOS3. We observed that recombinant TGFβ1

Figure 9. (See previous page). Liver infiltrating neutrophils display N2-polarization in ATP7B-KO mice and *atp7b*^{-/-} zebrafish. (A) Flow cytometric analysis of N1 (CD11b+Ly6G+NOS2+) and N2 (CD11b+Ly6G+CD206+) neutrophil populations in total CD11b+Ly6G+ cells derived from the livers of wild-type and ATP7B-KO mice at 6, 8, 16, and 24 weeks of age. (B) Flow cytometric quantification of CD11b+Ly6G+ neutrophils from wild-type and ATP7B-KO mice livers at 6, 8, 16, and 24 weeks of age. (C) Flow cytometric quantification of liver N1 and N2 neutrophils from wild-type and ATP7B-KO mice at 6, 8, 16, and 24 weeks of age. (B and C) n = 5–6 mice/group; unpaired 2-tailed *t* test. **P* < .05, ***P* < .01, and ****P* < .001. (D) Tracking of neutrophil movement within and surrounding the liver area in wild-type and mutant fish. Selected neutrophils were tracked based on 2-hour time-lapse videos. (E) Representative images of nuclear patterns after Giemsa staining in sorted neutrophils from wild-type and mutant fish. Scale bar: 100 μm. WT, wild-type.

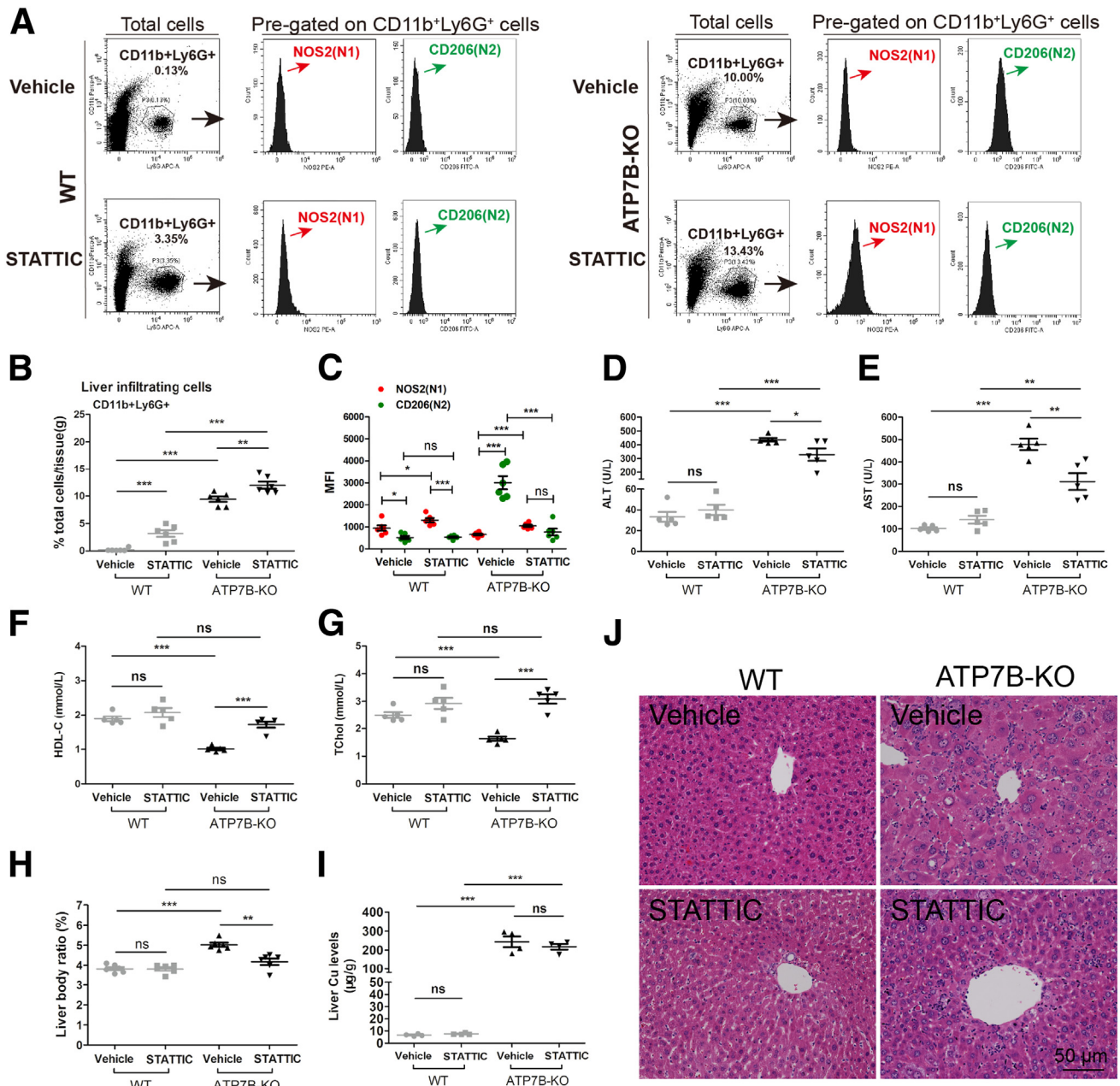


Figure 10. Ablating STAT3 in ATP7B-KO mice reduces liver N2-neutrophil polarization and alleviates liver pathology. (A) Flow cytometric analysis of N1 (CD11b+Ly6G+NOS2+) and N2 (CD11b+Ly6G+CD206+) neutrophil population in total CD11b+Ly6G+ cells derived from the livers of wild-type and ATP7B-KO mice treated with/without STATTIC. (B) Flow cytometric quantification of CD11b+Ly6G+ neutrophils from wild-type and ATP7B-KO mice livers treated with/without STATTIC. (C) Flow cytometric quantification of liver N1 and N2 neutrophils from wild-type and ATP7B-KO mice treated with/without STATTIC. (B and C) $n = 6$ mice/group; unpaired 2-tailed t test. $*P < .05$, $**P < .01$, and $***P < .001$. Serum activities of (D) ALT, (E) AST, (F) HDL-C, and (G) Tchol in wild-type and ATP7B-KO mice treated with/without STATTIC. $n = 5$ mice/group. $*P < .05$, $**P < .01$, $***P < .001$. (H) Liver body ratio in wild-type and ATP7B-KO mice treated with/without STATTIC. $n = 6$ mice/group. $**P < .01$, $***P < .001$. (I) Liver Cu content in wild-type and ATP7B-KO mice treated with/without STATTIC. $n = 4$ mice/group. $***P < .001$. (J) Representative H&E images in liver sections from wild-type and ATP7B-KO mice treated with/without STATTIC. Scale bar: 50 μ m. WT, wild-type.

treatment significantly skewed neutrophils toward the N2 type (*Arg2*, *CD206*, and *Ym1*) (Figure 15A). Down-regulated N2-associated markers were observed in neutrophils treated with TGF β 1 plus 5-aza or TGF β 1 plus STATTIC, while up-regulation of N1-associated markers (*CD95*, *Nos2*,

and *Ccl3*) was observed (Figure 15A). To examine the effect of neutrophil polarization, we harvested the conditioned medium to treat ATP7B-KO human hepatocellular carcinomas G2 (HepG2) cells, in which a whole knockout of exon 2 in the *ATP7B* gene was observed, which was a previously

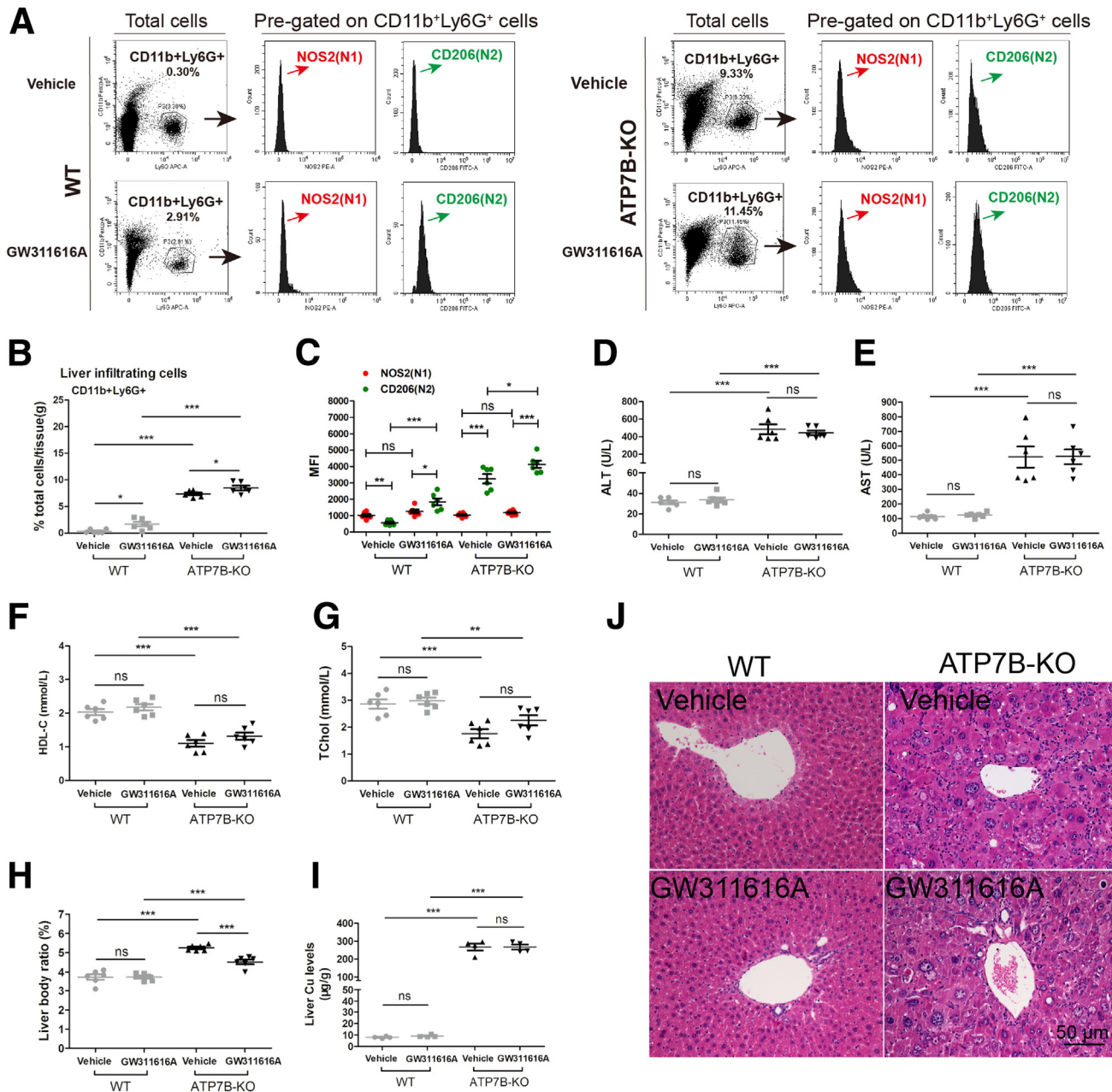


Figure 11. Pharmacologic inhibition of neutrophil elastase in ATP7B-KO mice increases liver N2-neutrophil polarization and aggravates liver pathology. (A) Flow cytometric analysis of N1 (CD11b+Ly6G+NOS2+) and N2 (CD11b+Ly6G+CD206+) neutrophil population in total CD11b+Ly6G+ cells derived from the livers of wild-type and ATP7B-KO mice treated with/without GW311616A. (B) Flow cytometric quantification of CD11b+Ly6G+ neutrophils from wild-type and ATP7B-KO mice livers treated with/without GW311616A. (C) Flow cytometric quantification of liver N1 and N2 neutrophils from wild-type and ATP7B-KO mice treated with/without GW311616A. (D) ALT, (E) AST, (F) HDL-C, and (G) TChol in wild-type and ATP7B-KO mice treated with/without GW311616A. (H) Liver body ratio in wild-type and ATP7B-KO mice treated with/without GW311616A. (I) Liver Cu content in wild-type and ATP7B-KO mice treated with/without GW311616A. (J) Representative H&E images in liver sections from wild-type and ATP7B-KO mice treated with/without GW311616A. Scale bar: 50 μ m. WT, wild-type.

established cellular model of Wilson's disease.²⁰ We found that epithelial-mesenchymal-transition markers (*E-cadherin*, *Epcam*, and *Keratin 18*) were down-regulated significantly in ATP7B-KO HepG2 cells upon treatment with conditioned medium from recombinant TGF β 1-treated bone

marrow neutrophils, but up-regulated in ATP7B-KO HepG2 cells upon treatment with conditioned medium from recombinant TGF β 1 plus 5-aza-treated or recombinant TGF β 1 plus STATTIC-treated bone marrow neutrophils (Figure 15B). To examine whether TGF β 1 promotes STAT3

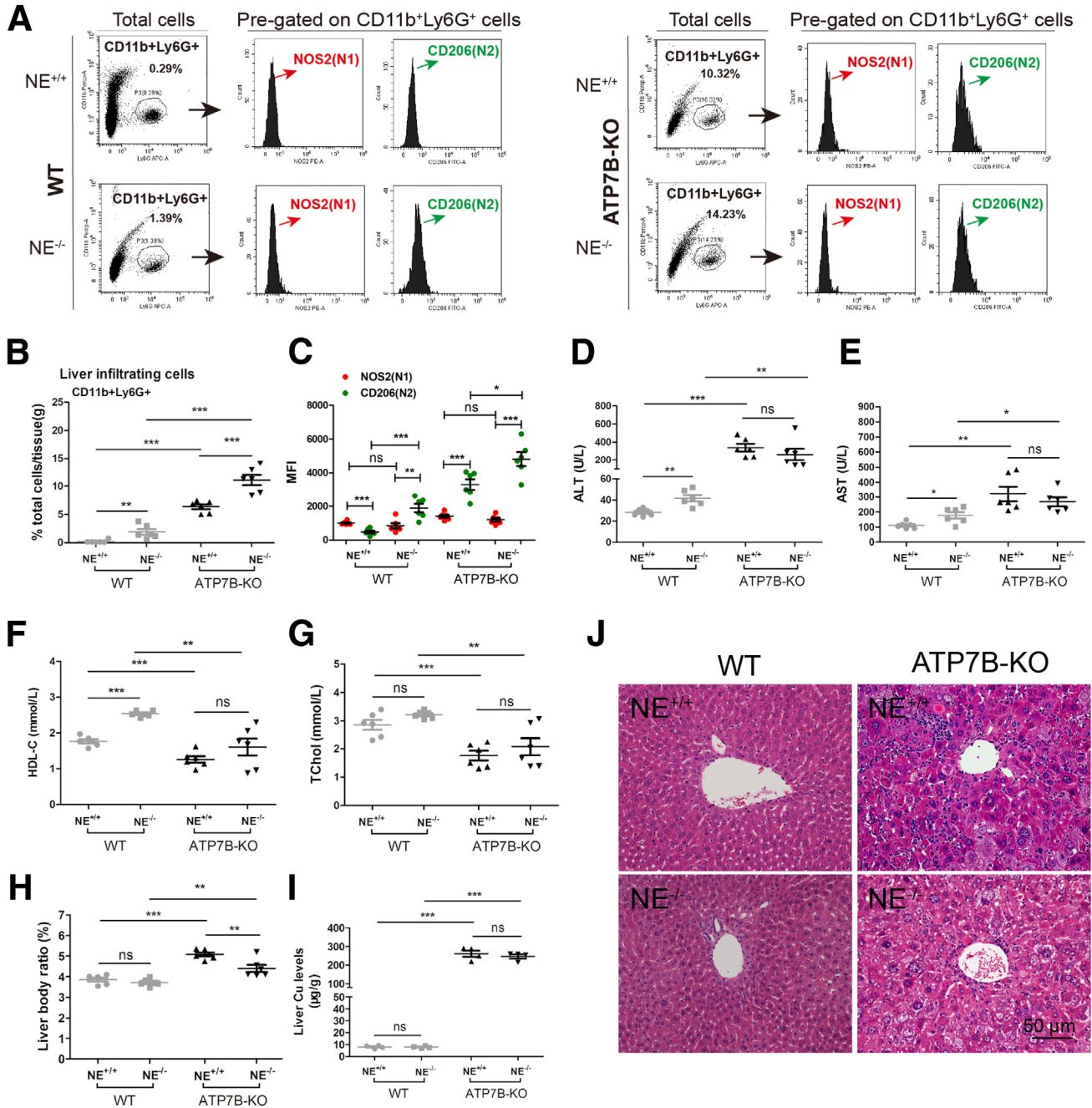


Figure 12. Genetic inhibition of neutrophil elastase in ATP7B-KO mice increases liver N2-neutrophil polarization and aggravates liver pathology. (A) Flow cytometric analysis of N1 (CD11b+Ly6G+NOS2+) and N2 (CD11b+Ly6G+CD206+) neutrophil populations in total CD11b+Ly6G+ cells derived from the livers of wild-type and ATP7B-KO mice with/without genetic deletion of neutrophil elastase. (B) Flow cytometric quantification of CD11b+Ly6G+ neutrophils from wild-type and ATP7B-KO mice livers with/without genetic deletion of neutrophil elastase. (C) Flow cytometric quantification of liver N1 and N2 neutrophils from wild-type and ATP7B-KO mice with or without genetic deletion of neutrophil elastase. (B and C) n = 6 mice/group; unpaired 2-tailed *t* test. **P* < .05, ***P* < .01, and ****P* < .001. Serum activities of (D) ALT, (E) AST, (F) HDL-C, and (G) TChol in wild-type and ATP7B-KO mice with/without genetic deletion of neutrophil elastase. n = 6 mice/group. **P* < .05, ***P* < .01, and ****P* < .001. (H) Liver body ratio in wild-type and ATP7B-KO mice with/without genetic deletion of neutrophil elastase. n = 6 mice/group. ***P* < .01, ****P* < .001. (I) Liver Cu content in wild-type and ATP7B-KO mice with/without genetic deletion of neutrophil elastase. n = 4 mice/group. ****P* < .001. (J) Representative H&E images in liver sections from wild-type and ATP7B-KO mice with/without genetic deletion of neutrophil elastase. Scale bar: 50 µm. WT, wild-type.

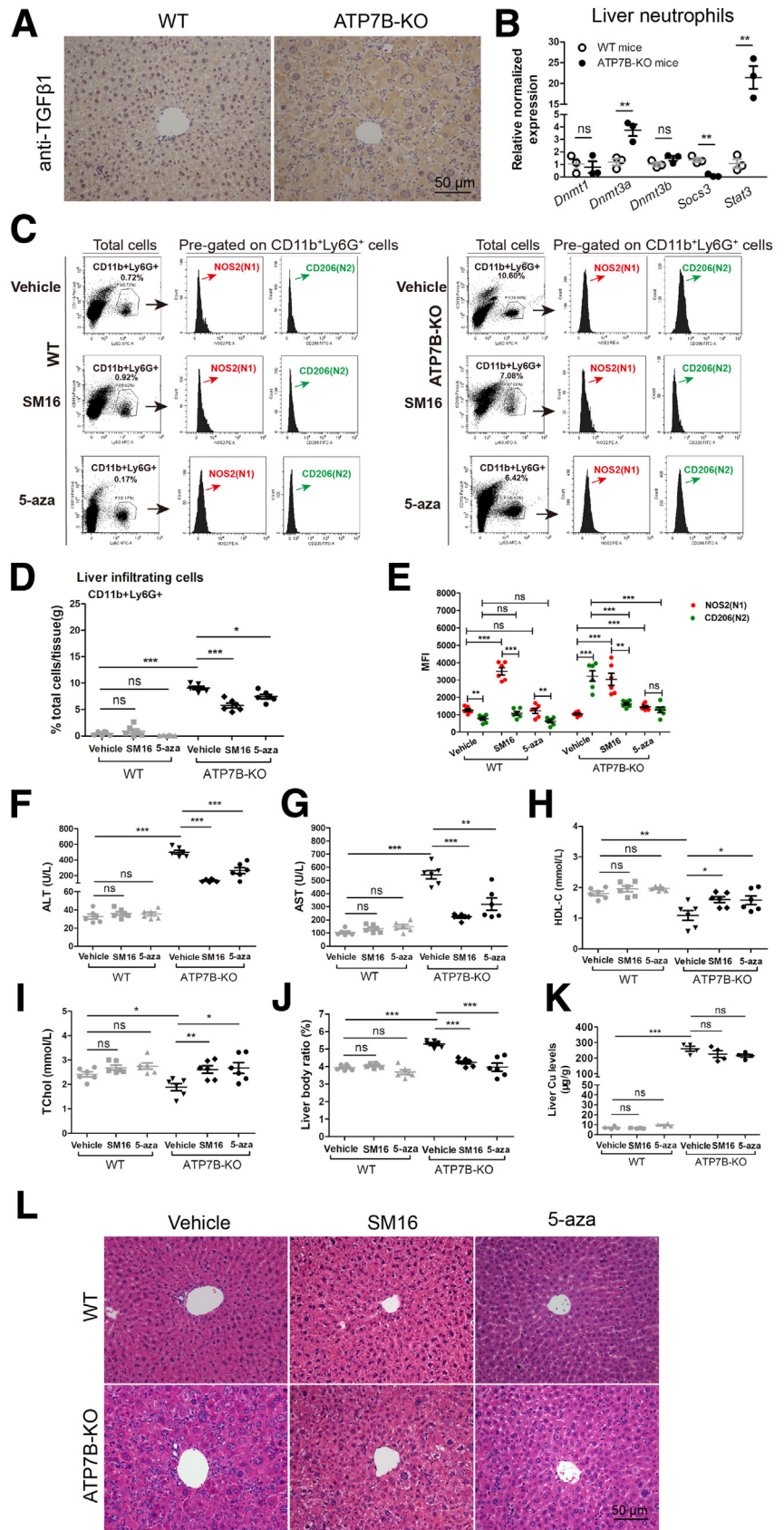


Figure 13. Inhibition of TGFβ1 signaling or DNA methylation in ATP7B-KO mice decreases liver N2-neutrophil polarization and improves liver pathology. (A) Representative immunohistochemical staining images of anti-TGFβ1 in wild-type and ATP7B-KO mice livers. Scale bar: 50 μm. (B) qPCR of gene expression changes in *Dnmt1*, *Dnmt3a*, *Dnmt3b*, *Scos3*, and *Stat3* in wild-type and ATP7B-KO mice liver neutrophils. n = 3 sets of neutrophils pooled from 2~3 mice. ***P* < .01. (C) Flow cytometric analysis of N1 (CD11b+Ly6G+NOS2+) and N2 (CD11b+Ly6G+CD206+) neutrophil population in total CD11b+Ly6G+ cells derived from the livers of wild-type and ATP7B-KO mice treated with/without SM16 or 5-aza. (D) Flow cytometric quantification of CD11b+Ly6G+ neutrophils from wild-type and ATP7B-KO mice livers treated with/without SM16 or 5-aza. (E) Flow cytometric quantification of liver N1 and N2 neutrophils from wild-type and ATP7B-KO mice treated with/without SM16 or 5-aza. (D and E) n = 6 mice/group, unpaired 2-tailed *t* test. **P* < .05, ***P* < .01, and ****P* < .001. Serum activities of (F) ALT, (G) AST, (H) HDL-C, and (I) TChol in wild-type and ATP7B-KO mice treated with/without SM16 or 5-aza. n = 6 mice/group. **P* < .05, ***P* < .01, and ****P* < .001. (J) Liver body ratio in wild-type and ATP7B-KO mice treated with/without SM16 or 5-aza. n = 6 mice/group. ****P* < .001. (K) Liver Cu content in wild-type and ATP7B-KO mice treated with/without SM16 or 5-aza. n = 4 mice/group. ****P* < .001. (L) Representative H&E images in liver sections from wild-type and ATP7B-KO mice treated with/without SM16 or 5-aza. Scale bar: 50 μm. WT, wild-type.

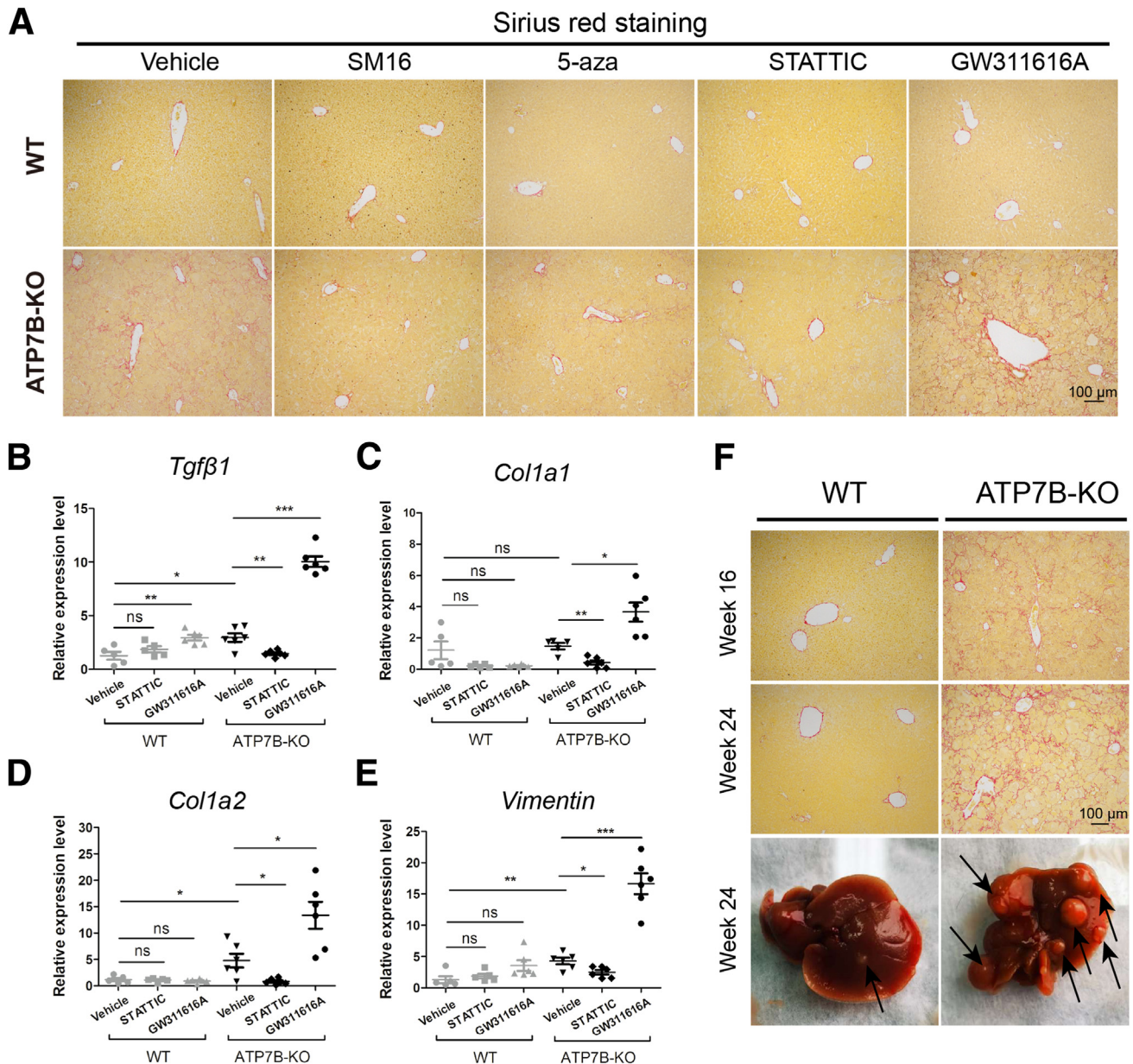


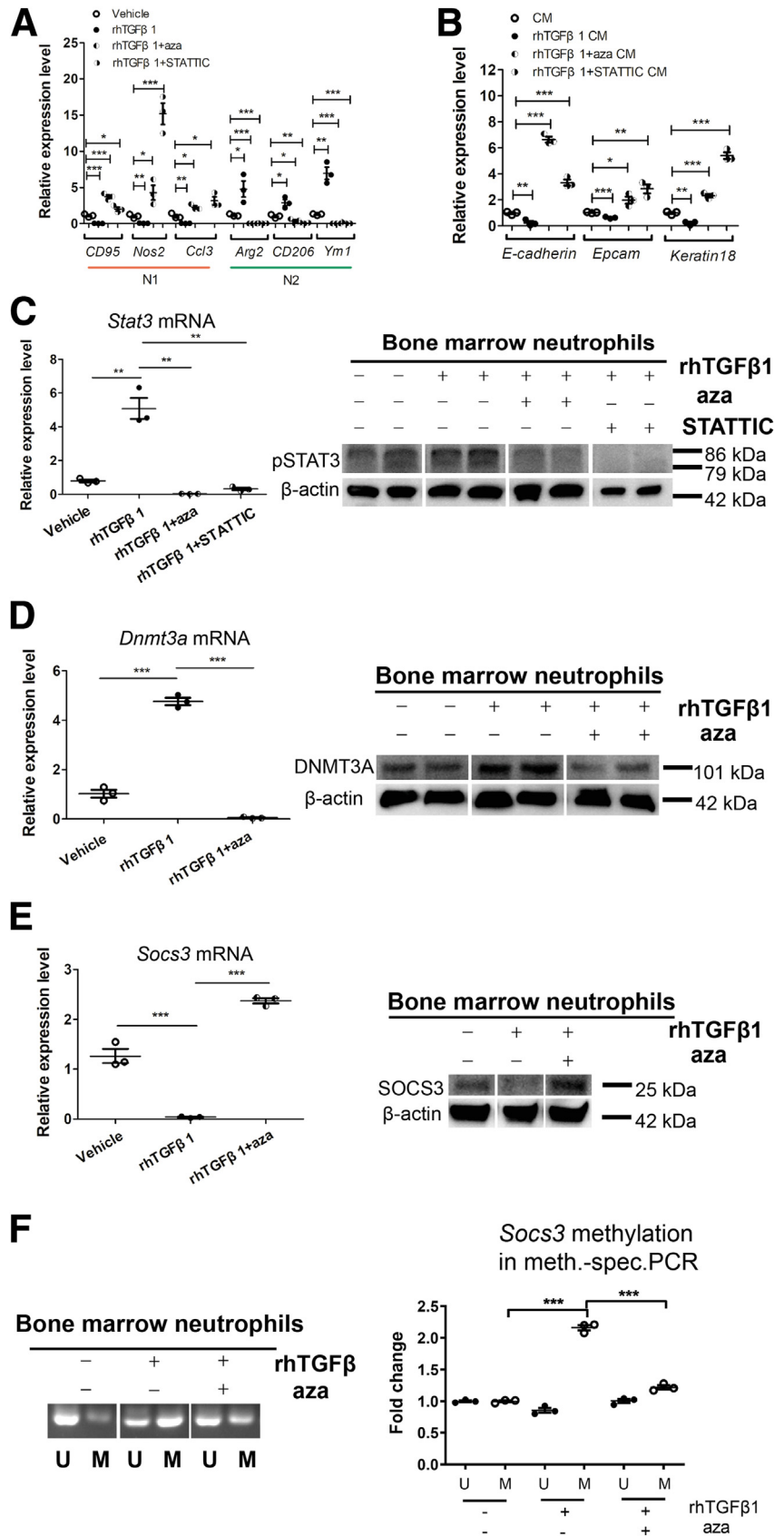
Figure 14. The effect of N2 neutrophils on liver fibrosis in ATP7B-KO mice. (A) Representative images of Sirius red staining in paraffin-embedded liver sections from vehicle-, SM16-, 5-aza-, STATTIC-, or GW311616A-treated mice. Scale bar: 100 μ m. qPCR of fibrogenic genes in (B) *Tgfβ1*, (C) *Col1a1*, (D) *Col1a2*, and (E) *vimentin* in wild-type and ATP7B-KO mice liver upon vehicle, STATTIC, or GW311616A treatment. $n = 5\sim 6$ mice/group. * $P < .05$, ** $P < .01$, and *** $P < .001$. (F) Upper panels: Representative images of Sirius red staining in paraffin-embedded liver sections from 16-week-old and 24-week-old wild-type and ATP7B-KO mice. Scale bar: 100 μ m. Lower panel: Macroscopic liver pathology in 24-week-old wild-type and ATP7B-KO mice. WT, wild-type.

expression by regulating DNMT3A expression to silence suppressor of cytokine signaling 3 (SOCS3) in neutrophil polarization, qPCR and Western blot analyses were performed. We found that the expression of *Stat3* was increased in bone marrow neutrophils upon recombinant TGF β 1 treatment and decreased upon TGF β 1 plus 5-aza treatment or TGF β 1 plus STATTIC treatment in bone marrow neutrophils (Figure 15C). The expression of *Dnmt3a* also was increased upon recombinant TGF β 1 treatment and decreased upon TGF β 1 plus 5-aza treatment

in bone marrow neutrophils (Figure 15D). The expression of *Socs3* was decreased upon recombinant TGF β 1 treatment and increased upon TGF β 1 plus 5-aza treatment in bone marrow neutrophils (Figure 15E). To directly demonstrate hypermethylation of the promoter region of the *Socs3* gene in neutrophils, we performed methylation-specific PCR. The ratio of methylated to unmethylated DNA was higher in bone marrow neutrophils treated with recombinant TGF β 1, and this ratio was abrogated in the presence of 5-aza (Figure 15F). Together, these data suggest that TGF β 1

Figure 15. The TGFβ1–DNMT3A–STAT3 signaling axis mediates N2-neutrophil polarization in Wilson's disease.

(A) qPCR of gene expression changes in N1 markers (*CD95*, *Nos2*, and *Ccl3*) and N2 markers (*Arg2*, *CD206*, and *Ym1*) in bone marrow neutrophils treated with vehicle, rhTGFβ1 (Recombinant Human TGF-beta 1), rhTGFβ1 plus 5-aza, or rhTGFβ1 plus STATTIC. n = 3 sets of bone marrow neutrophils pooled from 2~3 mice. **P* < .05, ***P* < .01, and ****P* < .001. (B) qPCR of gene expression changes in epithelial-mesenchymal-transition markers (*E-cadherin*, *Epcam*, and *Keratin 18*) in ATP7B-KO HepG2 cells treated with culture medium from vehicle-, rhTGFβ1-, rhTGFβ1 plus 5-aza-, or rhTGFβ1 plus STATTIC-treated bone marrow neutrophils. n = 3 sets of ATP7B-KO HepG2 cells. **P* < .05, ***P* < .01, and ****P* < .001. (C) The expression changes of *Stat3* in bone marrow neutrophils treated with vehicle, rhTGFβ1, rhTGFβ1 plus 5-aza, or rhTGFβ1 plus STATTIC. *Left panel*: qPCR of *Stat3* mRNA expression. n = 3 sets of bone marrow neutrophils pooled from 2~3 mice. ***P* < .01, and ****P* < .001. *Right panel*: Western blot of pSTAT3 protein expression. β-actin was used as internal control. n = 2 sets of bone marrow neutrophils pooled from 2~3 mice. (D) The expression changes of *Dnmt3a* in bone marrow neutrophils treated with vehicle, rhTGFβ1, rhTGFβ1 plus 5-aza, or rhTGFβ1 plus STATTIC. *Left panel*: qPCR of *Dnmt3a* mRNA expression. n = 3 sets of bone marrow neutrophils pooled from 2~3 mice. ****P* < .001. *Right panel*: Western blot of DNMT3A protein expression. β-actin was used as internal control. n = 2 sets of bone marrow neutrophils pooled from 2~3 mice. (E) The expression changes of *Socs3* in bone marrow neutrophils treated with vehicle, rhTGFβ1, or rhTGFβ1 plus 5-aza. *Left panel*: qPCR of *Socs3* mRNA expression. n = 3 sets of bone marrow neutrophils pooled from 2~3 mice. ****P* < .001. *Right panel*: Western blot of SOCS3 protein expression. β-actin was used as internal control. n = 3 technical replicates/group. (F) Methylation-specific PCR in *Socs3* promoter in bone marrow neutrophils treated with vehicle, rhTGFβ1, or rhTGFβ1 plus 5-aza. *Left panel*: Representative images of methylation-specific PCR in *Socs3* promoter. *Right panel*: Quantification of band levels by ImageJ. M, methylated; U, unmethylated. n = 3 sets of bone marrow neutrophils pooled from 2~3 mice. ****P* < .001. CM, culture medium.



promotes N2-neutrophil polarization by inducing DNA methylation to silence SOCS3 and thus facilitate STAT3 expression.

To determine the source of TGFβ1 as well as the in vivo targeting of SM16, we performed immunofluorescence staining in liver sections from SM16-treated mice or vehicle-

treated mice. As shown in Figure 16A, increased expression of TGFβ1 was detected in albumin-positive liver hepatocytes in vehicle-treated ATP7B-KO mice, and this increased expression of TGFβ1 in ATP7B-KO mouse liver hepatocytes was significantly inhibited upon SM16 treatment. Then, we isolated liver hepatocytes from SM16-treated mice or

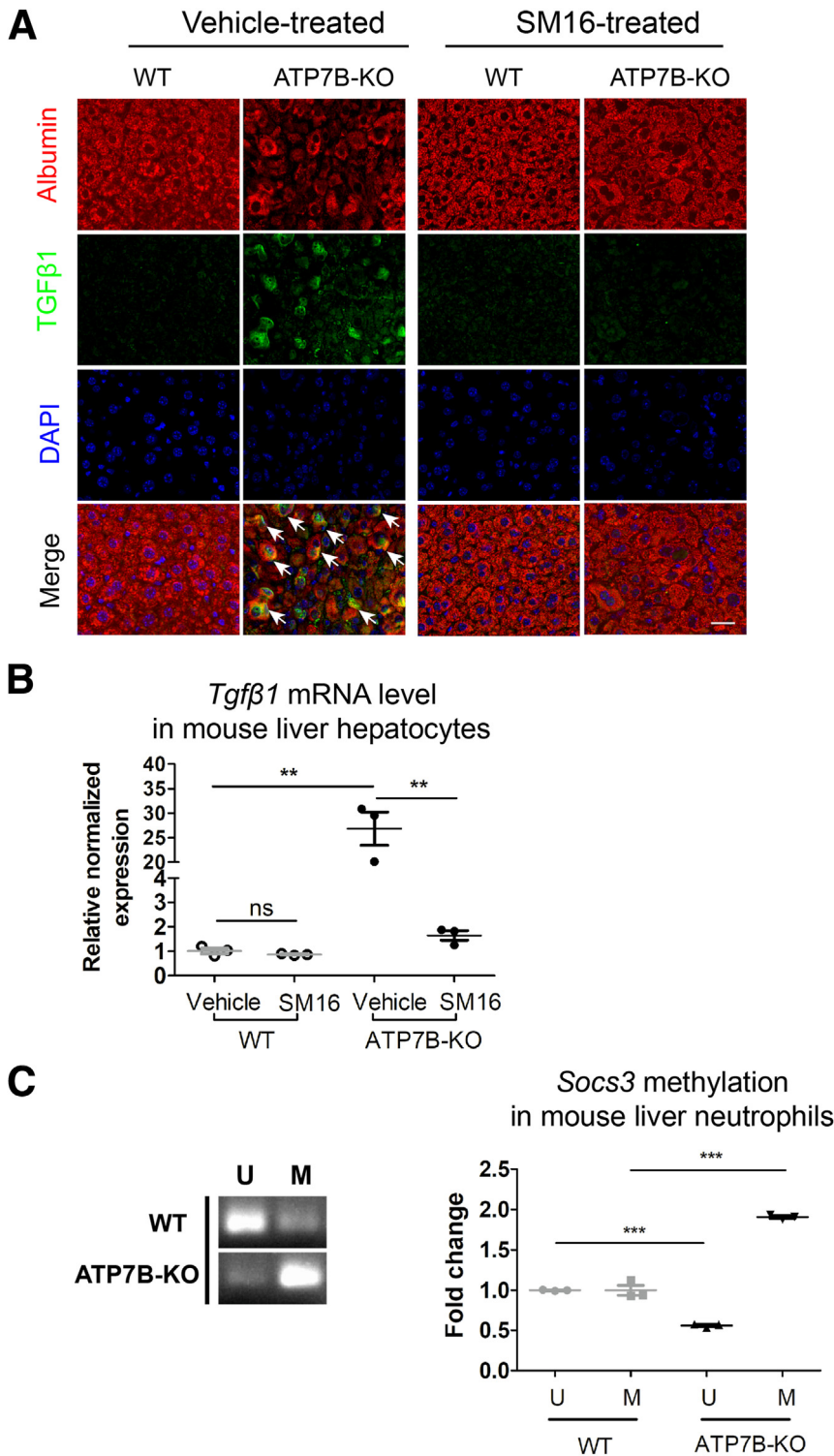


Figure 16. TGFβ1 is highly increased in hepatocytes in ATP7B-KO mice. (A) Formalin-fixed mouse liver tissue sections from SM16-treated or vehicle-treated wild-type and ATP7B-KO mice were subjected to immunofluorescence staining of anti-TGFβ1 and anti-albumin. Representative images of TGFβ1 (green), albumin (red), and nuclei (blue) are shown. Arrows indicate TGFβ1-positive hepatocytes. Scale bar: 40 μm. (B) qPCR of mRNA levels of *Tgfβ1* in liver hepatocytes isolated from wild-type and ATP7B-KO mice upon SM16 or vehicle treatment. n = 3 sets of liver hepatocytes pooled from 2~3 mice. **P < .01. (C) Methylation-specific PCR in *Socs3* promoter in liver neutrophils from wild-type and ATP7B-KO mice. Left panel: Representative images of methylation-specific PCR in *Socs3* promoter. Right panel: Quantification of band levels by ImageJ. M, methylated; U, unmethylated. n = 3 sets of liver neutrophils pooled from 2~3 mice. ***P < .001. DAPI, 4',6-diamidino-2-phenylindole; WT, wild-type.

vehicle-treated mice to detect the messenger RNA (mRNA) level of *Tgfb1* using qPCR. As shown in **Figure 16B**, the mRNA level of *Tgfb1* was increased in liver hepatocytes from vehicle-treated ATP7B-KO mice, and this increase in liver hepatocytes from ATP7B-KO mice was significantly inhibited upon SM16 treatment. Meanwhile, to provide in vivo evidence of epigenetic changes in liver neutrophils from ATP7B-KO mutants, methylation-specific PCR was performed to determine hypermethylation of the promoter region of the *Socs3* gene in liver neutrophils from ATP7B-KO mice and wild-type mice. As shown in **Figure 16C**, the ratio of methylated to unmethylated DNA was higher in liver neutrophils from ATP7B-KO mice. We also performed immunofluorescence staining in liver sections and qPCR in isolated liver neutrophils from STAT3-treated mice or vehicle-treated mice to detect the source of STAT3 as well as the in vivo targeting of STAT3. As shown in **Figure 17A**, increased expression of phosphorylated-STAT3 was detected in Ly6G-positive liver neutrophils in vehicle-treated ATP7B-KO mice, and STAT3 treatment specifically inhibited the expression of pSTAT3 in liver neutrophils in ATP7B-KO mice; the mRNA level of *Stat3* was increased in

liver neutrophils isolated from vehicle-treated ATP7B-KO mice, and this increase in ATP7B-KO mouse liver neutrophils was significantly inhibited upon STAT3 treatment (**Figure 17B**). Furthermore, the long-term effects of targeting N2 neutrophils on the liver injury phenotype were detected in ATP7B-KO mice and wild-type mice 4 months after STAT3 treatment. As shown in **Figure 18**, body weight, liver body ratio, and biochemical parameters, such as ALT, AST, HDL-C, and TChol, all were improved in ATP7B-KO mice 4 months after STAT3 treatment. Moreover, pathologic phenotypes in ATP7B-KO mouse livers with karyomegaly, cytomegaly, inflammation, necrosis, and liver fibrosis also were alleviated in ATP7B-KO mice 4 months after STAT3 treatment.

To provide evidence that the earlier-described findings we have reported in male mice are comparable with those in females, we isolated liver-infiltrated neutrophils and performed flow cytometry analysis in female ATP7B-KO mice and wild-type mice. As shown in **Figure 19**, liver-infiltrated neutrophils (CD11b+Ly6G+) were increased in female ATP7B-KO mice compared with wild-type control mice (**Figure 19A and B**). Among total liver-infiltrated

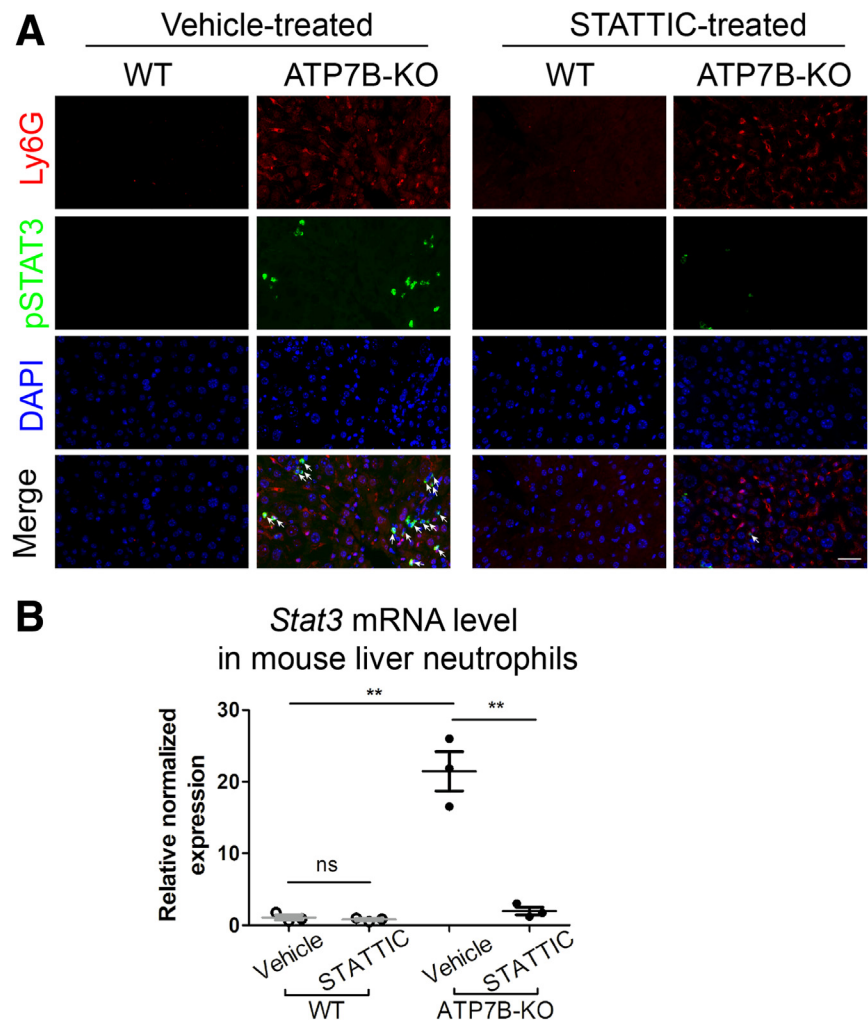


Figure 17. STAT3 is highly increased in liver neutrophils in ATP7B-KO mice. (A) Formalin-fixed mouse liver tissue sections from STAT3-treated or vehicle-treated wild-type and ATP7B-KO mice were subjected to immunofluorescence staining of anti-pSTAT3 and anti-Ly6G. Representative images of pSTAT3 (green), Ly6G (red), and nuclei (blue) are shown. Arrows indicate pSTAT3-positive liver neutrophils. Scale bar: 40 μ m. (B) qPCR of mRNA levels of *Stat3* in liver neutrophils isolated from wild-type and ATP7B-KO mice upon STAT3 or vehicle treatment. n = 3 sets of liver neutrophils pooled from 2~3 mice. **P < .01. DAPI, 4',6-diamidino-2-phenylindole; WT, wild-type.

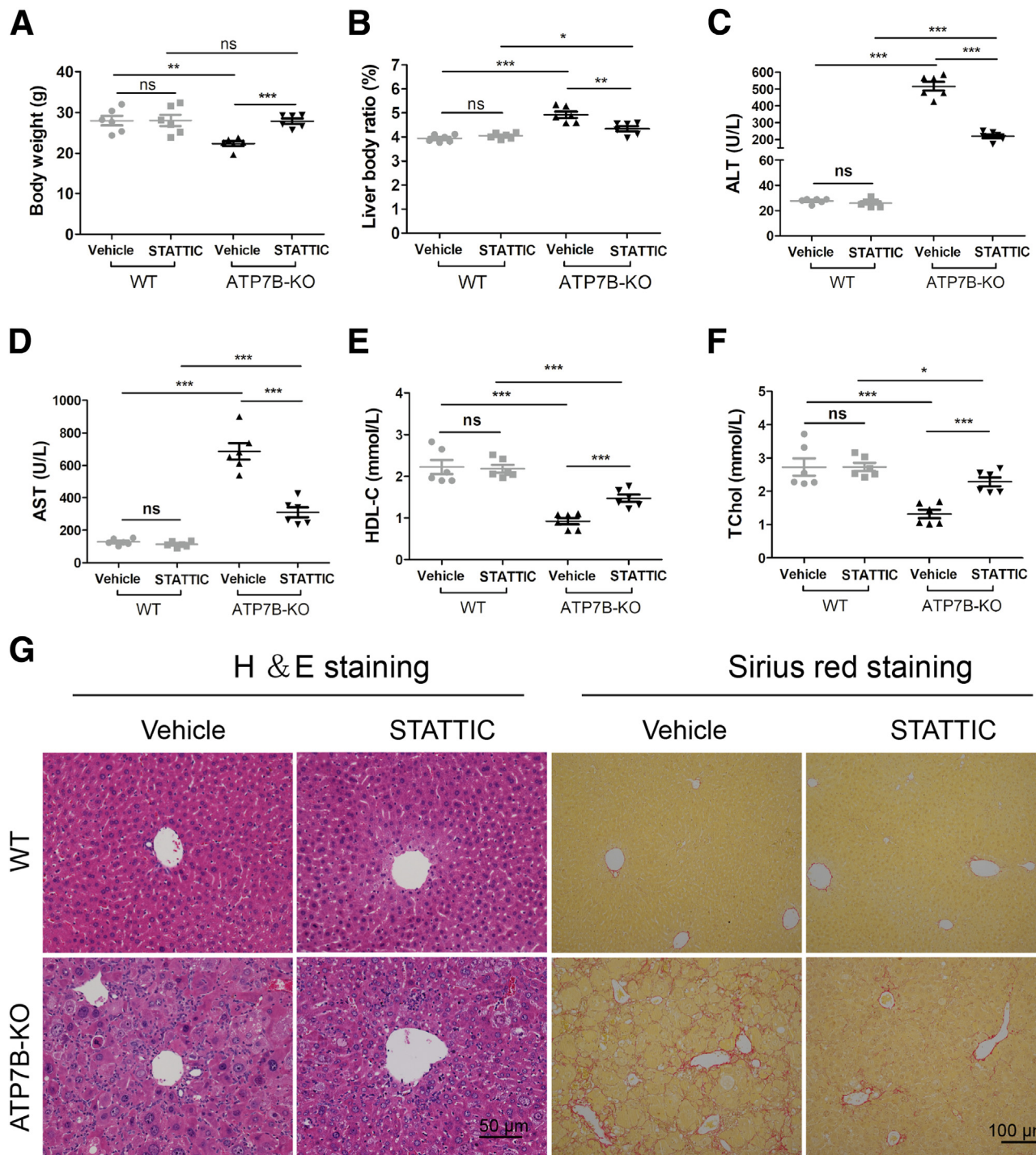
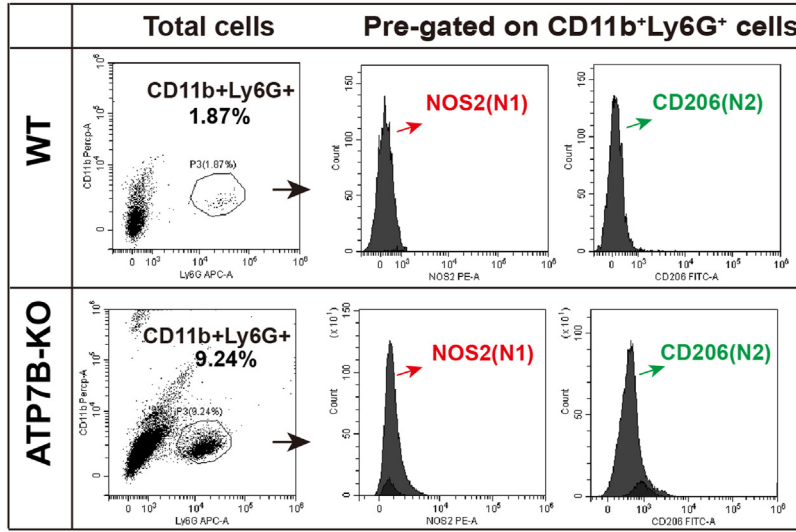


Figure 18. The long-term effect of N2 neutrophils on liver injury phenotype in ATP7B-KO mice. (A and B) Body weight and liver body ratio in wild-type and ATP7B-KO mice 4 months after STATTIC treatment. $n = 6$ mice/group. $*P < .05$, $**P < .01$, and $***P < .001$. Serum activities of (C) ALT, (D) AST, (E) HDL-C, and (F) TChol in wild-type and ATP7B-KO mice 4 months after STATTIC treatment. $n = 6$ mice/group. $*P < .05$, $***P < .001$. (G) Pathologic changes in liver sections from wild-type and ATP7B-KO mice 4 months after STATTIC treatment. *Left panel:* Representative H&E images in paraffin-embedded liver sections. Scale bar: 50 μm . *Right panel:* Representative images of Sirius red staining in paraffin-embedded liver sections. Scale bar: 100 μm . WT, wild-type.

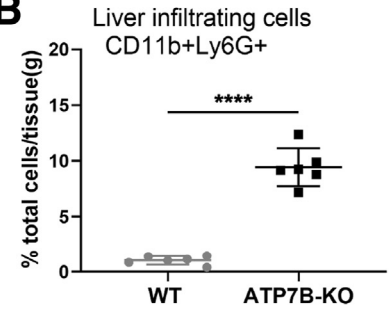
neutrophils, more N2-type neutrophils (CD206+) were detected than N1-type neutrophils (NOS2+) in female ATP7B-KO mice (Figure 19A and C). Furthermore, H&E staining of liver sections showed widespread inflammation

and necrosis in female ATP7B-KO mice at 16 weeks of age (Figure 19D, upper panel), and Sirius red staining showed liver fibrosis in female ATP7B-KO mice (Figure 19D, lower panel). Increased expression of *Tgfb1* in isolated liver

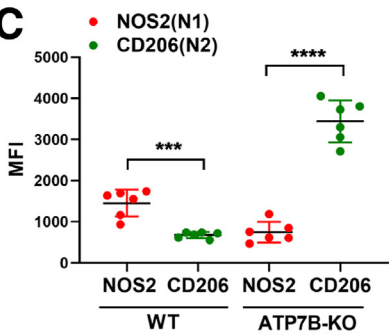
A



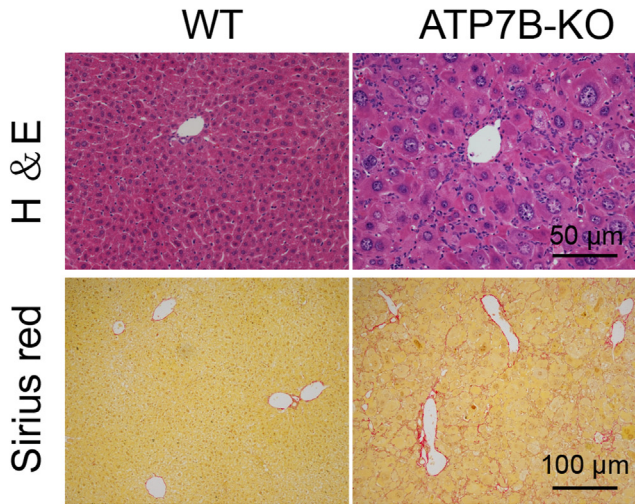
B



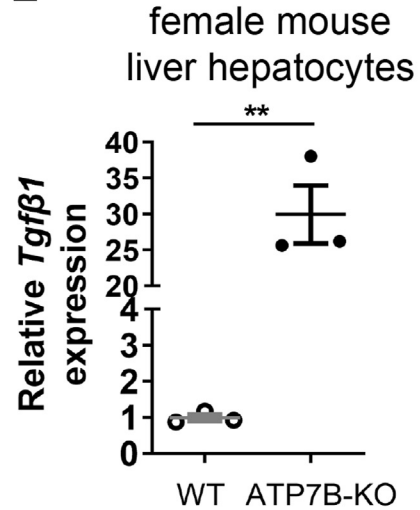
C



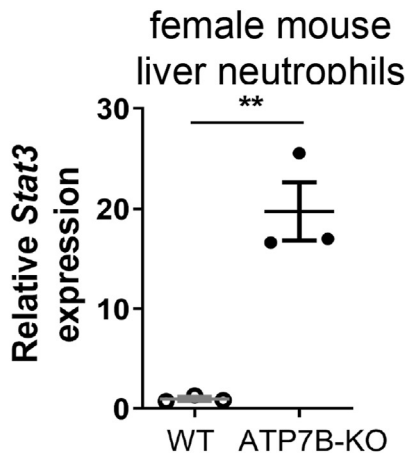
D



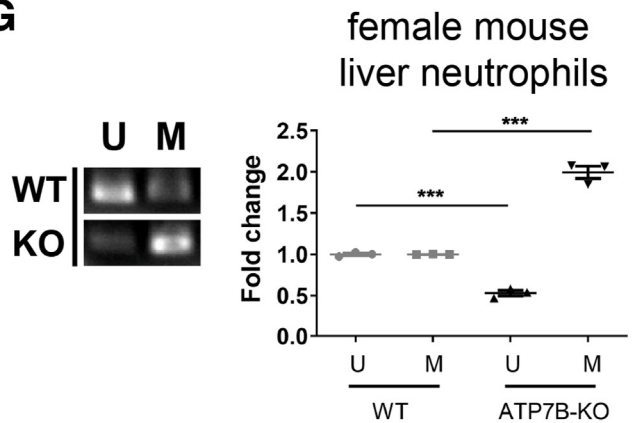
E



F



G



hepatocytes was detected in female ATP7B-KO mice (Figure 19E). Meanwhile, the mRNA level of *Stat3* was increased in female ATP7B-KO mouse liver neutrophils (Figure 19F). In addition, we performed methylation-specific PCR experiments to determine hypermethylation of the promoter region of the *Socs3* gene in liver neutrophils from female *Atp7b* mutants. As shown in Figure 19G, the ratio of methylated to unmethylated DNA was higher in liver neutrophils from female ATP7B-KO mice. Together, these data showed that the findings we have reported in male mice are comparable with those in females.

Discussion

We show by multiple experiments that DNMT3A/STAT3 signaling causes the pro-polarization effects of TGF β 1 on neutrophils and that targeted inhibition of TGF β 1, DNMT activity, or STAT3 ameliorates neutrophil polarization and prevents liver disease progression in Wilson's disease. The experimental results are summarized as follows: (1) neutrophils infiltrate into the liver and contribute to liver pathogenesis in a fish model revealed by live imaging and pharmacologic modulation; (2) infiltrated neutrophils display distinct gene transcriptional profiles and migratory patterns as well as ring-formed nuclei characteristic of N2 neutrophils in a fish model, and N2-type neutrophils also are observed in a mouse model; (3) pharmacologic inhibition of STAT3, DNMT, or TGF β 1 signaling alleviates N2-neutrophil polarization and prevents liver fibrosis development in a mouse model; and (4) the activation of STAT3 in neutrophil polarization occurs in a TGF β -dependent manner by hypermethylation of the *Socs3* promoter in isolated bone marrow neutrophils and in Wilson's disease mice. Taken together, these findings showed that the TGF β 1-DNMT3A/STAT3 signaling axis is required for neutrophil polarization, thus resulting in liver disease progression in Wilson's disease.

TGF β 1 is the most potent chemoattractant for neutrophils.²⁷ In our study, we observed that the total liver-infiltrated neutrophils were reduced in SM16-treated ATP7B-KO mice (Figure 13D). In addition to the chemoattractant effect on neutrophils, we further showed that TGF β 1 displays a pro-polarization effect on liver neutrophils in Wilson's disease (Figure 13E). Mature human TGF β 1 shares 100% amino acid identity with pig, dog, and cow TGF β 1, and 99% aa identity with mouse, rat, and horse TGF β 1. This shows

that TGF β 1 exerts cross-species activity.²⁸ Based on our anti-TGF β 1 immunohistochemical/immunofluorescence staining results from mouse liver sections (Figures 13A and 16), these data suggest that TGF β 1 comes from hepatocytes in Wilson's disease liver. Changes in intracellular copper trafficking from the cytoplasm to the nucleus initiate transcriptome remodeling in Wilson's disease hepatocytes.²⁹ We propose that in Wilson's disease, accumulating copper in hepatocytes initiates transcriptome remodeling, leading to increased expression of TGF β 1, which is a critical chemoattractant for neutrophils, and, furthermore, TGF β 1 polarizes the recruited neutrophils to the N2 phenotype to promote liver disease progression. This represents a novel mechanism in the pathogenesis of Wilson's disease.

Tyagi et al¹⁴ examined microarray data of N1/N2 neutrophils (GSE101584) and cross-referenced them with the transcription factor database and found that STAT3 is essential for N2-neutrophil polarization. Consistent with this observation, we showed that *Stat3* expression is increased significantly in ATP7B-KO mouse liver neutrophils (Figures 13B and 17), and inhibition of STAT3 activity using the known STAT3 inhibitor STATTIC reduced N2-neutrophil polarization and improved liver morphology and function in Wilson's disease (Figure 10). Although there was no decrease in the Cu level in STATTIC-treated mutant livers (Figure 10I), no decreases in the Cu levels were observed in SM16- or 5-aza-treated mutant livers (Figure 13K). According to our speculation, neutrophils are not involved in the hepatic handling of copper, and the reason for hepatic copper accumulation in Wilson's disease is copper transporter-ATP7B deficiency, which cannot be alleviated by N2 inhibition. Although STATTIC-treated mutant livers showed a dramatic improvement in architecture, some multinucleated cells and swollen hepatocytes remained (Figure 10J). Collectively, these data suggested that N2 neutrophils contribute partly to the pathogenesis of Wilson's disease, and pharmacologic modulation of N2 neutrophil activity should be explored as a supplementary approach to improve liver function in Wilson's disease. Nevertheless, our study improves the understanding of neutrophil biology in the pathogenesis and development of neutrophil-related disease.

We observed that the expression of *Dnmt3a* but not *Dnmt1* or *Dnmt3b* was increased significantly in ATP7B-KO mouse liver neutrophils (Figure 13B). DNMT3A operates as a de novo DNMT, while DNMT1 serves to maintain

Figure 19. (See previous page). The N2 neutrophils and liver injury phenotype also were observed in female ATP7B-KO mice. (A) Flow cytometric analysis of N1 (CD11b+Ly6G+NOS2+) and N2 (CD11b+Ly6G+CD206+) neutrophil populations in total CD11b+Ly6G+ cells derived from the livers of female wild-type and ATP7B-KO mice. (B) Flow cytometric quantification of CD11b+Ly6G+ neutrophils from female wild-type and ATP7B-KO mice livers. (C) Flow cytometric quantification of liver N1 and N2 neutrophils from female wild-type and ATP7B-KO mice. (B and C) n = 6 mice/group; unpaired 2-tailed *t* test. ****P* < .001, *****P* < .0001. (D) Pathologic changes in liver sections from female wild-type and ATP7B-KO mice at age 16 weeks. *Upper panel:* Representative H&E images in paraffin-embedded liver sections. *Scale bar:* 50 μ m. *Lower panel:* Representative images of Sirius red staining in paraffin-embedded liver sections. *Scale bar:* 100 μ m. (E) qPCR of mRNA levels of *Tgf β 1* in liver hepatocytes isolated from female wild-type and ATP7B-KO mice. n = 3 sets of liver hepatocytes pooled from 2~3 mice. ***P* < .01. (F) qPCR of mRNA levels of *Stat3* in liver neutrophils isolated from female wild-type and ATP7B-KO mice. n = 3 sets of liver neutrophils pooled from 2~3 mice. ***P* < .01. (G) Methylation-specific PCR in *Socs3* promoter in liver neutrophils from female wild-type and ATP7B-KO mice. *Left panel:* Representative images of methylation-specific PCR in *Socs3* promoter. *Right panel:* Quantification of band levels by ImageJ. M, methylated; U, unmethylated. n = 3 sets of liver neutrophils pooled from 2~3 mice. ****P* < .001. WT, wild-type.

preexisting DNA methylation marks.³⁰ DNA methylation is one important approach to silence SOCS3 expression.^{31,32} Our data suggest that the stimulatory effect of TGF β 1 on *Socs3* promoter methylation is mediated by the induction of DNMT3A in neutrophils. However, Mordaunt et al³³ did not see any evidence of hypermethylation of DNA to suppress SOCS3 in human Wilson's disease liver biopsy specimens by whole-genome bisulfite sequencing. Hepatocytes are the primary component of the liver and account for 60% of the total cell number.³⁴ Thus, the hypermethylation of DNA in liver neutrophils may be ignored by analyzing whole human liver pieces. In addition, whether prolonged incubation with TGF β 1 also induces the expression of DNMT1 in neutrophils needs to be determined. Treatment with 5-aza does not cause random DNA demethylation.³⁵ Hence, 5-aza may not promote a higher risk of adverse events, imposing a promising therapeutic effect in Wilson's disease.

Uneven sex distribution among Wilson's disease patients was only a theoretical bias; however, females more often develop acute hepatic failure.² Thus, we performed most of our experiments in male mice to avoid the interference of sex distribution in statistical analysis. It has been reported that heterozygotes do not have normal copper metabolism when compared with patients with Wilson's disease³⁶; thus, we chose wild-type siblings, not heterozygotes, as the reference control in all our experiments. The existing rodent models of Wilson's disease all recapitulate human hepatic Wilson's disease but lack a convincing neurologic phenotype.³⁷ Our established zebrafish models present hepatic defects, including steatosis and fibrosis, as well as behavioral defects, such as abnormal swimming ability, which are features of human Wilson's disease.²⁰ Human beings with Wilson's disease may present with neurologic defects, often some degree of movement disturbances. The *atp7b*^{-/-} fish displayed altered swimming behavior, which may be parallel to human dystonia. We observed that hepatic and behavioral defects were aggravated by stimulation of liver-infiltrated neutrophils in our fish model (Figures 4 and 5). However, we also observed that PR 39 treatment changed the swimming behavior in non-Wilson zebrafish with no statistically significant differences in swimming distance and velocity between groups (Figure 5). Whether the behavior defects result from liver defects through communication between the liver and brain or N2 neutrophils are involved in the brain remains unknown. The type of rodent animal model selected in our study was ATP7B-KO mice, which are characterized by extensive regenerative changes in the liver, with the development of fibrotic nodes but not cancer. The best model to study would be Long evans cinnamon rats, which is actually a model of spontaneous HCC development after surviving fulminant hepatitis in the presence of massive copper accumulation.³⁷ However, except for *Atp7b* deficiency, additional mutations in the gene involved in melatonin production and a further unspecified mutation responsible for cinnamon coat color have been reported in Long evans cinnamon rats.³⁸

Together, we elucidate the role and machinery of neutrophil heterogeneity in the hepatic pathogenesis of Wilson's disease. We propose that accumulating Cu in

hepatocytes initiates transcriptome remodeling, leading to the release of TGF β 1, with consequent polarization of the recruited neutrophils through the TGF β 1-DNMT3A/STAT3 signaling axis; therefore, the formation of N2 neutrophils drives liver disease progression and fibrosis/cirrhosis development. In human Wilson's disease, most liver biopsy specimens show moderate to severe steatosis, variable degrees of portal and/or lobular inflammation, and fibrosis eventually progressing to cirrhosis.³⁹ Pharmacologic targets of TGF β 1, DNMT or STAT3 reduce N2-neutrophil polarization, and improve liver functions of transaminase levels, as well as alleviate liver inflammation and fibrosis, which all are indicators of effective therapeutics. These preliminary studies on murine/fish/cellular models of Wilson's disease provide an alternative therapeutic strategy for Wilson's disease and will contribute to future clinical applications.

Materials and Methods

Animals

The *atp7b*^{-/-} fish recapitulate human Wilson's disease by exposing 5-day-old fish larvae to Cu dissolved in fish water, which is a fish model for Wilson's disease previously established by our laboratory.²⁰ The *ATP7B*^{-/-} mice (here indicated as ATP7B-KO mice, JAX stock #032624; Jackson Laboratories) were generated on the hybrid of heterozygous animals of the C57BL/6;129S6 background and genotyped at 2 ~ 3 weeks of age as described.⁴⁰ Double-knockout mice (*ATP7B*^{-/-}*NE*^{-/-}) were generated by crossing *ATP7B*^{+/-} mice with genetic neutrophil elastase-deficient mice (indicated as *NE*^{-/-} mice). Pharmacologic treatments were performed in male mice from 8 weeks of age to 16 weeks of age, as indicated. All animals were bred and manipulated according to the guidelines approved by the Ethical Committee of Hangzhou Normal University.

Animal Treatment

LPS (L4391; Sigma), FPR A14 (2826; Tocris), and PR 39 (1947; Tocris) were first dissolved in dimethyl sulfoxide as stocks and then diluted in fish water and used to expose fish larvae for 24 hours at final concentrations of 1 μ g/mL, 2.5 μ mol/L, and 50 nmol/L, respectively.⁴¹ Fish then were collected for live imaging and neutrophil isolation. Mice at 8 weeks of age were treated with STATTIC¹⁴ (2 mg/kg intraperitoneally, 3 times/wk), GW311616A²⁵ (2 mg/kg intragastrically, 3 times/wk), SM16⁴² (2 mg/kg intragastrically, 3 times/wk), or 5-aza²⁶ (0.5 mg/kg intraperitoneally, 2 times/wk) until 16 weeks of age, as indicated. Blood and liver tissues were collected from mice that were killed for biochemical analysis, histologic analysis, and neutrophil isolation. The animal experiments were approved by the Ethical Committee for Animal Welfare of Hangzhou Normal University (approval number: 2021-1031).

Live Imaging

The *atp7b*^{-/-} fish were crossed with *Tg(lyz:DsRED2)* fish or *Tg(mpx:EGFP)* fish for the production of offspring with a *lyz*⁺ or *mpx*⁺ background. After Cu or pharmacologic exposure, the fish were anesthetized and imaged on a Nikon

Eclipse Ti confocal microscope for infiltrating *lyz*⁺ or *mpx*⁺ neutrophil number count and liver size analysis.

Movement Tracking

Fish movement tracking for swimming pattern analysis was performed as we described previously.²⁰ For neutrophil movement tracking, time-lapse confocal microscopy was conducted on wild-type and mutant larvae embedded in 3% low-melting-point agarose, and the time-lapse videos were used for neutrophil tracking with multiparticle tracking by Imaris (Bitplane, version 9.3.1).

Fish Neutrophil Isolation

Fluorescence-activated cell sorting (FACS) was performed to isolate neutrophils from zebrafish larvae as previously described.⁴³ Briefly, the *lyz*⁺/*atp7b*^{-/-} fish and the control *lyz*⁺/*atp7b*^{+/+} fish were collected and treated with 0.05% trypsin-EDTA for 30 minutes with careful pipetting up and down. The dissociation was stopped by adding 10% heat-inactivated fetal bovine serum and then centrifuged at 200 × *g* for 7 minutes. The supernatant was discarded, and FACSmax cell dissociation solution (T200100; AMS Biotechnology) was added and centrifuged at 310 × *g* for 1 minute. The supernatant was discarded, and the remaining supernatant was resuspended in FACSmax cell dissociation solution again. The resulting cell suspension was filtered through a 40- μ m cell strainer, and the *lyz*⁺ neutrophils were sorted by Beckman moFlo Astrios EQ for further analysis.

Giemsa Staining

Giemsa staining was performed in FACS-isolated neutrophils. After fixation in methanol for 3 minutes, the neutrophils then were stained with Giemsa solution (G1015; Solarbio) for 20 minutes at room temperature. The images were taken on a Nikon Eclipse 80i microscope for cytologic analyses.

RNA Sequencing

Total RNA was isolated by TRIzol from FACS-sorted neutrophils. The Qubit & Nanodrop 2000 and an Agilent 2100 Bioanalyzer were used to detect the concentration and integrity to ensure that the RNA samples met the quality requirements of transcriptome sequencing. The Switching mechanism at 5' end of the RNA transcript (SMART) method was used to amplify mRNA. The constructed complementary DNA (cDNA) library was quality checked by the Qubit and Agilent 2100 Bioanalyzer. The Illumina HiSeq platform was used to sequence the library based on a 2 × 150 base pair double-terminal sequencing strategy. The sequencing results were analyzed by DESeq2 (Illumina) to identify differentially expressed genes between each group. Kyoto Encyclopedia of Genes and Genomes pathway enrichment was performed by KOBAS 3.0 (Center for Bioinformatics, Peking University). Protein and protein interaction networks were analyzed by Sting.

qPCR

Total RNA was isolated with TRIzol (Life Technologies) or the Quick-RNA MicroPrep Kit (R1050; Zymo Research) as indicated according to the manufacturer's instructions, and then transcribed into cDNA using a HiScript II first-strand cDNA synthesis kit (R211-01; Vazyme) via the manufacturer's instructions. Reverse-transcription qPCR was performed using ChamQ universal SYBR qPCR master mix (Vazyme, Q711) according to the manufacturer's instructions. Total RNA in mouse liver neutrophils or bone marrow neutrophils was isolated from a pool of neutrophils separated from 2 ~ 3 mice. *β -actin* or *EFL1- α* was used as an internal control. Primer sequences of the genes of interest are listed in Table 1.

Western Blot and Immunofluorescence Staining

Protein was extracted using RIPA lysis buffer from mouse bone marrow neutrophils, as indicated. The extracted protein was resolved by sodium dodecyl sulfate-polyacrylamide gel electrophoresis and then transferred to polyvinylidene difluoride membranes. The membrane was blocked with 5% bovine serum albumin (BSA) for 1 hour at room temperature and then incubated with primary antibodies overnight at 4°C. The primary antibodies used were as follows: anti-pSTAT3 (9145; Cell Signaling Technology), anti-SOCS3 (ab16030; Abcam), and anti-DNMT3A (ab2850; Abcam). After horseradish-peroxidase-conjugated secondary antibody incubation for 1 hour at room temperature, the protein bands were visualized using ECL ultra Western horseradish-peroxidase substrate (WBULS0100; Millipore). For immunofluorescence staining, fish larvae were fixed in 4% paraformaldehyde overnight at 4°C and then rinsed with phosphate-buffered saline (PBS) and double-distilled water. The samples then were treated with acetone at -20°C for 10 minutes to penetrate the tissue. After blocking with mix of phosphate-buffered saline, dimethyl sulfoxide, Triton X-100 (PBBDT) solution (composed of 1× PBS, 1% BSA [w/v], 1% dimethyl sulfoxide [v/v], and 0.5% Triton X-100 (Sigma) [v/v]) with 2% normal goat serum for 1 hour at room temperature, the samples were stained with TGF- β 1 rabbit polyclonal antibody (21898-1-AP; Proteintech) overnight at 4°C. After rinsing with PBBDT 3 times, the samples were incubated with goat anti-rabbit IgG (H+L) Alex Flour 488 (A-11008; Invitrogen) and 4',6-diamidino-2-phenylindole (C0060, 1 μ g/mL; Solarbio) for 6 hours at room temperature. Images were taken on a Nikon Eclipse Ti confocal microscope. The average fluorescence intensity was quantified by ImageJ software (version 1.42; National Institutes of Health) and expressed as arbitrary units.

Mouse Liver Neutrophil Isolation

Mouse liver was grinded and passed through a 70- μ m cell strainer (BD Falcon) in PBS, and the cell suspension was centrifuged at 400 rpm for 5 minutes at 4°C to pellet the hepatocytes and cell debris. The supernatant-enriched liver leukocytes then were centrifuged at 1700 rpm for 10

Table 1. Primers Used to Amplify Target Gene Expressions for qPCR

Gene	Primers, 5'-3'	Gene	Primers, 5'-3'
<i>zpparα</i>	F: CGTCGTCAGGTGTTTACGGT R: AGGCACTTCTGGAATCGACA	<i>zpparγ</i>	F: GGTTTCATTACGGCGTTCCAC R: TGGTTCACGTCACCTGGAGAA
<i>zsrebp1</i>	F: CATCCACATGGCTCTGAGTG R: CTCATCCACAAAGAAGCGGT	<i>zucp2</i>	F: GAGCTTTGCTTCTGTACGCA R: ACGAAACCCCTCTTCTTTG
<i>zil1β</i>	F: TGGCGAACGTCATCCAAG R: GGAGCACTGGGCGACGCATA	<i>zil6</i>	F: GCACGGAAGATGTCTAACGC R: AAGGATAGGGAAGTGCTGGATG
<i>ztnfα</i>	F: GCTTATGAGCCATGCAGTGA R: TGCCAGTCTGTCTCTTCT	<i>zil12a</i>	F: TCTCCAGTTCTCTCTCCA R: AAACCAGCAAACAAGTCC
<i>znfκb</i>	F: GAAGCATTGAGGCTCGGTGA R: CAGGTCTGTGGTCCCTTTC	<i>zil13ra1</i>	F: TGGAGACCTGCTGTTGAT R: CCATTGTAAGTGCCGTTG
<i>zccl19b</i>	F: CGAATCCCTCAGAAAGTG R: GCTCGGAAATGGTGC	<i>zccl39.1</i>	F: TGGTGCTCTTCTGCTC R: TCGTGGTCAAGTGCTGA
	F: ACCCACCGAGTGCCTCA		F: ATCAATGCCACAAACCTG
<i>zlyz</i>	R: TTTCAGCCCGTCCATTTT	<i>zmpx</i>	R: TTGGATGCACCAAGAAGT
<i>mDnmt1</i>	F: TCGACAGTGACACCCTT R: TCTACAACCTCTGCGTTTCTT	<i>mDnmt3a</i>	F: GGTCATGTGGTTCGGAGAT R: GACTTCGTAGATGGCTTTGC
<i>mDnmt3b</i>	F: CGCCTCAAGACAAATAGC R: CAGAGCCCACCTCAAAG	<i>mSocs3</i>	F: GCGGATTCTACTGGAGCG R: GGATGCGTAGGTTCTTGGTC
<i>mStat3</i>	F: GAGAACCTCCAGGACGACT R: AGGGCTGTGAGCATCTGT	<i>mTgfβ1</i>	F: CAGACATTCGGGAAGCAG R: CTCAGCGTATCAGTGGG
<i>mCol1a1</i>	F: GGCGGTTCCAGGTCCAATG R: GCAATCCACGAGCACCCT	<i>mCol1a2</i>	F: GCGGACTCTGTTGCTGCTT R: CCTGCGGGACCCCTTTGT
<i>mVimentin</i>	F: TTGAACGGAAAGTGGAAATC R: AGGTCAGGCTTGGAAACG	<i>mCD95</i>	F: GCACAGAAGGGAAGGAGT R: CCAGGAGAATCGCAGTAG
<i>mNos2</i>	F: ACCAGGAGATGTTGAACTATGT R: GTGGCTCTGACCCGTGAA	<i>mCcl3</i>	F: AGCCAGGTGTCAATTTTCC R: GCATTGAGTCCAGGTCA
<i>mArg2</i>	F: AATACATAATACAGGGTTGC R: AGTAGGAAGGTGGTCATAGA	<i>mCD206</i>	F: GCTCGGGACTCTGGATTG R: CAGGCTCTGATGATGGACTT
<i>mYm1</i>	F: CTAATCCTCAGAACCGTCAGATA R: TTTACGCATTTCTTCAACA	<i>hE-cadherin</i>	F: ACGCATTGCCACATACAC R: ACCTTCCATGACAGACCC
<i>hEpcam</i>	F: CTGGCCGTAAACTGCTTT R: CATTCTGCCTTCATCACC	<i>hKeratin18</i>	F: GCTGAGATCGCCACCTAC R: CCACTTTCCATCCACTA
<i>zEFL1-α</i>	F: TACTTCTCAGGCTGACTGTG R: ATCTTCTTGATGTATGCGCT	<i>mβ-actin</i>	F: GACAGGATGCAGAAGGAGATTAC R: GCTGGAAGGTGGACAGTGAG

F, forward; h, HepG2 cells; m, mouse; R, reverse; z, zebrafish.

minutes at 4°C. The pellet was resuspended in 15 mL 35% Percoll (P8370; Solarbio) and centrifuged at 2400 rpm for 5 minutes at 4°C. The resulting pellet was resuspended in 5 mL Red blood cell lysis buffer (R1010; Solarbio) and centrifuged at 2400 rpm for 5 minutes at 4°C. The resulting cells were washed with 15 mL PBS and centrifuged at 1700 rpm for 5 minutes at 4°C. The cells were collected in PBS with 2% BSA for further analysis.

Flow Cytometry

Neutrophils isolated from mouse livers were resuspended in PBS with 2% BSA and then stained fluorescently with Peridinin-Chlorophyll-Protein Complex anti-mouse/human CD11b antibody (101230, 1:100; BioLegend) and Allophycocyanin anti-mouse Ly6G antibody (127614, 1:500; BioLegend) for 30 minutes at 4°C. After washing with PBS twice, 4% Paraformaldehyde was added to fix the cells for 15 minutes at room temperature. Then, 90% methanol (v/v

in 1× PBS) was added to permeate the cells on ice for 10 minutes. The neutrophils then were stained fluorescently with Phycoerythrin anti-NOS2 (Inducible Nitric oxide synthase 2) antibody (696806, 1:200; BioLegend) and fluorescein isothiocyanate anti-mouse CD206 (macrophage mannose receptor) antibody (141704, 1:500; BioLegend). Data were acquired on a CytoFLEX Flow Cytometer (Beckman Coulter).

Histologic Analysis and Biochemical Analysis

A piece of mouse liver (left lobe) was fixed with 4% paraformaldehyde for embedding the following day, and the remaining liver tissue was flash-frozen and stored at -80°C. For embedding, the liver piece was dehydrated successively in 75%, 80%, 85%, 95%, and 100% ethanol solutions at room temperature and then immersed in dimethyl benzene for 20 minutes at room temperature. Paraffin immersion was performed at 65°C for 3 hours, followed by embedding

at 4°C. A rotary microtome was used to cut the piece into 4- μ m sections. The sections then were deparaffinized and stained with H&E or Picro Sirius red for histologic analysis or with anti-TGF- β 1 antibody (21898-1-AP; Proteintech), anti-albumin antibody (SAB3500217; Sigma), anti-Ly6G antibody (ab238132; Abcam), or anti-pSTAT3 antibody (9145; Cell Signaling Technology) for gene expression analysis. Histologic analysis of zebrafish liver tissue was performed as previously reported.²⁰ For experiments requiring biochemical analysis, blood was obtained from the killed mice by retro-orbital bleeding at the indicated time points, and the serum was isolated from whole blood by centrifugation at 3500 rpm for 15 minutes at room temperature. For all experiments, the mice were randomly assigned, and the sample size was chosen based on statistical analysis.

Copper Content Determination

For fish liver copper measurement, a total of approximately 1000 fish larvae were collected, and head/tail tissues were removed to determine accumulated liver tissue Cu levels as previously described.²⁰ Briefly, after the indicated pharmacologic treatment, the required amount of fish trunk tissues (100–200 mg) was collected to measure liver copper levels. For mouse liver copper measurement, a piece of liver tissue (approximately 100 mg) from the left lobe each mouse was collected. All collected samples were digested with HNO₃ and Hydrofluoric acid, and then incubated with HClO₄. Cu levels were measured using an Agilent 7500 inductively coupled plasma mass spectrometer. At least 3 biological replicates were measured for each group. Data are expressed as copper levels normalized to tissue weight.

Mouse Bone Marrow Neutrophil Isolation and Chemical Treatment

Bone marrow neutrophils were isolated from C57BL/6 mice at 12–14 weeks of age as previously reported.⁴⁴ In brief, femurs and tibias were separated from the mice that were killed. The ends of the bones were cut to expose the cavity, and a 25-gauge needle on a 5-mL syringe containing ice-cooled RPMI 1640 medium with 10% fetal bovine serum and 1% penicillin–streptomycin was used to rinse marrow cells from the bones. After filtration through a 70- μ m cell strainer (BD Falcon), cells were collected by centrifugation at 3000 rpm for 4 minutes and subsequently resuspended in RPMI medium. The marrow neutrophils were purified by density gradient centrifugation. A stock solution of Percoll was prepared in 8.5% NaCl at a ratio of 9:1 (v/v; Percoll: 8.5% NaCl). Two 3-mL Percoll discontinuous density gradients (78%, 65% with 0.85% NaCl) were prepared in a 15-mL polypropylene conical tube. The marrow suspension was layered on top of the Percoll gradient and centrifuged at 800 \times g for 35 minutes without a brake. Bone marrow neutrophils formed a band at the interface of the 65% and 78% Percoll layers. This band was carefully aspirated and mixed with 3 mL PBS in a 15-mL conical tube, centrifuged at 1000 rpm for 3 minutes, washed twice with PBS, and then

Table 2. Primer Sequences Used for Methylation-Specific PCR in Mouse *Socs3* Promoter

	Sequence, 5'-3'
Methylation-specific <i>Socs3</i>	F: TTTTGTGTTTGTGTAATAATC
	R: TTTAAATATCTAAACTTTCCCGAT
Unmethylation-specific <i>Socs3</i>	F: TTTTGTGTTTGTGTAATAATTTG
	R: TTTAAATATCTAAACTTTCCAAT

lysed with 2 mL Red blood cell lysis buffer to remove red blood cells. The collected cells were resuspended in RPMI medium and counted by a hemocytometer. For chemical treatment, freshly isolated neutrophils pooled from 2–3 mice were cultured for 24 hours in RPMI medium in the presence of recombinant Human transforming growth factor beta1 (10 ng/mL; R&D Systems) with/without 5-aza (1 μ mol/L; Sigma) or STATTIC (1 μ mol/L; Sigma). For the inhibitor assay, neutrophils were pretreated with each inhibitor for 0.5 hours before TGF β 1 was added. To prepare conditioned medium, neutrophil-conditioned medium was harvested and then centrifuged to remove cells and debris at 3000 rpm for 10 minutes. The supernatant then was filtered through a 0.22- μ m filter and stored at –80°C for further use.

Methylation-Specific PCR

Genomic DNA was isolated from mouse bone marrow neutrophils or mouse liver neutrophils as indicated using the TIANGEN genomic DNA Extraction kit (DP304; TIANGEN) per the manufacturer's instructions. For methylation-specific PCR, approximately 800 ng genomic DNA was processed using the DNA Bisulfite Conversion Kit (DP215; TIANGEN) according to the manufacturer's instructions. The sequences of the primer pairs used for methylation- and nonmethylation-specific PCR are summarized in Table 2. The reaction mixture contained 50 ng bisulfite-converted DNA in a final volume of 20 μ L using a methylation-specific PCR kit (EM101; TIANGEN) according to the manufacturer's instructions. Each product was loaded onto a 1.5% agarose gel and visualized under ultraviolet illumination. Each band was quantified using ImageJ.

Statistical Analysis

Data are expressed as the means \pm SEM, and statistical significance between groups was compared using the Student 2-tailed *t* test. Differences with *P* < .05 were considered significant.

References

1. Czlonkowska A, Litwin T, Dusek P, et al. Wilson disease. *Nat Rev Dis Primers* 2018;4:21.
2. Ferenci P, Stremmel W, Czlonkowska A, et al. Age and sex but not ATP7B genotype effectively influence the

- clinical phenotype of Wilson disease. *Hepatology* 2019; 69:1464–1476.
3. Gerosa C, Fanni D, Congiu T, et al. Liver pathology in Wilson's disease: from copper overload to cirrhosis. *J Inorg Biochem* 2019;193:106–111.
 4. Medici V, Trevisan CP, D'Inca R, et al. Diagnosis and management of Wilson's disease: results of a single center experience. *J Clin Gastroenterol* 2006; 40:936–941.
 5. Weiss KH, Thurik F, Gotthardt DN, et al. Efficacy and safety of oral chelators in treatment of patients with Wilson disease. *Clin Gastroenterol Hepatol* 2013;11, 1028–1035.e1–2.
 6. Schilsky ML. Liver transplantation for Wilson's disease. *Ann N Y Acad Sci* 2014;1315:45–49.
 7. Fridlender ZG, Sun J, Kim S, et al. Polarization of tumor-associated neutrophil phenotype by TGF-beta: "N1" versus "N2" TAN. *Cancer Cell* 2009;16:183–194.
 8. Sagiv JY, Michaeli J, Assi S, et al. Phenotypic diversity and plasticity in circulating neutrophil subpopulations in cancer. *Cell Rep* 2015;10:562–573.
 9. Pylaeva E, Lang S, Jablonska J. The essential role of type I interferons in differentiation and activation of tumor-associated neutrophils. *Front Immunol* 2016; 7:629.
 10. Piccard H, Muschel RJ, Opendakker G. On the dual roles and polarized phenotypes of neutrophils in tumor development and progression. *Crit Rev Oncol Hematol* 2012;82:296–309.
 11. Shaul ME, Levy L, Sun J, et al. Tumor-associated neutrophils display a distinct N1 profile following TGFbeta modulation: a transcriptomics analysis of pro- vs. antitumor TANs. *Oncoimmunology* 2016;5: e1232221.
 12. Masucci MT, Minopoli M, Carriero MV. Tumor associated neutrophils. Their role in tumorigenesis, metastasis, prognosis and therapy. *Front Oncol* 2019;9:1146.
 13. Mihaila AC, Ciortan L, Macarie RD, et al. Transcriptional profiling and functional analysis of N1/N2 neutrophils reveal an immunomodulatory effect of S100A9-blockade on the pro-inflammatory N1 subpopulation. *Front Immunol* 2021;12:708770.
 14. Tyagi A, Sharma S, Wu K, et al. Nicotine promotes breast cancer metastasis by stimulating N2 neutrophils and generating pre-metastatic niche in lung. *Nat Commun* 2021;12:474.
 15. Denny MF, Yalavarthi S, Zhao W, et al. A distinct subset of proinflammatory neutrophils isolated from patients with systemic lupus erythematosus induces vascular damage and synthesizes type I IFNs. *J Immunol* 2010; 184:3284–3297.
 16. Cuartero MI, Ballesteros I, Moraga A, et al. N2 neutrophils, novel players in brain inflammation after stroke: modulation by the PPARgamma agonist rosiglitazone. *Stroke* 2013;44:3498–3508.
 17. Ma Y, Yabluchanskiy A, Iyer RP, et al. Temporal neutrophil polarization following myocardial infarction. *Cardiovasc Res* 2016;110:51–61.
 18. Meer van S, Man de RA, Berg van den AP, et al. No increased risk of hepatocellular carcinoma in cirrhosis due to Wilson disease during long-term follow-up. *J Gastroenterol Hepatol* 2015;30:535–539.
 19. Pfeifferberger J, Mogler C, Gotthardt DN, et al. Hepatobiliary malignancies in Wilson disease. *Liver Int* 2015; 35:1615–1622.
 20. Mi X, Li Z, Yan J, et al. Activation of HIF-1 signaling ameliorates liver steatosis in zebrafish *atp7b* deficiency (Wilson's disease) models. *Biochim Biophys Acta Mol Basis Dis* 2020;1866:165842.
 21. Yan C, Huo X, Wang S, et al. Stimulation of hepatocarcinogenesis by neutrophils upon induction of oncogenic *kras* expression in transgenic zebrafish. *J Hepatol* 2015;63:420–428.
 22. Shi J, Ross CR, Leto TL, Blecha F. PR-39, a proline-rich antibacterial peptide that inhibits phagocyte NADPH oxidase activity by binding to Src homology 3 domains of p47 phox. *Proc Natl Acad Sci U S A* 1996; 93:6014–6018.
 23. Kumar S, Dikshit M. Metabolic insight of neutrophils in health and disease. *Front Immunol* 2019;10:2099.
 24. Cui C, Chakraborty K, Tang XA, et al. Neutrophil elastase selectively kills cancer cells and attenuates tumorigenesis. *Cell* 2021;184:3163–3177.e21.
 25. Mansuy-Aubert V, Zhou QL, Xie X, et al. Imbalance between neutrophil elastase and its inhibitor alpha1-antitrypsin in obesity alters insulin sensitivity, inflammation, and energy expenditure. *Cell Metab* 2013;17:534–548.
 26. Dees C, Potter S, Zhang Y, et al. TGF-beta-induced epigenetic deregulation of SOCS3 facilitates STAT3 signaling to promote fibrosis. *J Clin Invest* 2020; 130:2347–2363.
 27. Reibman J, Meixler S, Lee TC, et al. Transforming growth factor beta 1, a potent chemoattractant for human neutrophils, bypasses classic signal-transduction pathways. *Proc Natl Acad Sci U S A* 1991;88:6805–6809.
 28. Derynck R, Miyazono K. The TGF-beta family. Cold Spring Harbor Laboratory Press, 2008:29.
 29. Ralle M, Huster D, Vogt S, et al. Wilson disease at a single cell level: intracellular copper trafficking activates compartment-specific responses in hepatocytes. *J Biol Chem* 2010;285:30875–30883.
 30. Jones PA. Functions of DNA methylation: islands, start sites, gene bodies and beyond. *Nat Rev Genet* 2012; 13:484–492.
 31. He B, You L, Uematsu K, et al. SOCS-3 is frequently silenced by hypermethylation and suppresses cell growth in human lung cancer. *Proc Natl Acad Sci U S A* 2003;100:14133–14138.
 32. Niwa Y, Kanda H, Shikauchi Y, et al. Methylation silencing of SOCS-3 promotes cell growth and migration by enhancing JAK/STAT and FAK signalings in human hepatocellular carcinoma. *Oncogene* 2005;24:6406–6417.
 33. Mordaunt CE, Kieffer DA, Shibata NM, et al. Epigenomic signatures in liver and blood of Wilson disease patients include hypermethylation of liver-specific enhancers. *Epigenetics Chromatin* 2019;12:10.
 34. Kumar S, Duan Q, Wu R, et al. Pathophysiological communication between hepatocytes and non-parenchymal cells in liver injury from NAFLD to liver fibrosis. *Adv Drug Deliv Rev* 2021;176:113869.

35. Tabolacci E, Mancano G, Lanni S, et al. Genome-wide methylation analysis demonstrates that 5-aza-2-deoxycytidine treatment does not cause random DNA demethylation in fragile X syndrome cells. *Epigenetics Chromatin* 2016;9:12.
36. Sandahl TD, Gormsen LC, Kjaergaard K, et al. The pathophysiology of Wilson's disease visualized: a human (64) Cu PET study. *Hepatology* 2022;75:1461–1470.
37. Reed E, Lutsenko S, Bandmann O. Animal models of Wilson disease. *J Neurochem* 2018;146:356–373.
38. Ahmed S, Deng J, Borjigin J. A new strain of rat for functional analysis of PINA. *Brain Res Mol Brain Res* 2005;137:63–69.
39. Pronicki M. Wilson disease - liver pathology. *Handb Clin Neurol* 2017;142:71–75.
40. Buiakova OI, Xu J, Lutsenko S, et al. Null mutation of the murine ATP7B (Wilson disease) gene results in intracellular copper accumulation and late-onset hepatic nodular transformation. *Hum Mol Genet* 1999;8:1665–1671.
41. Novoa B, Bowman TV, Zon L, Figueras A. LPS response and tolerance in the zebrafish (*Danio rerio*). *Fish Shellfish Immunol* 2009;26:326–331.
42. Fu K, Corbley MJ, Sun L, et al. SM16, an orally active TGF-beta type I receptor inhibitor prevents myofibroblast induction and vascular fibrosis in the rat carotid injury model. *Arterioscler Thromb Vasc Biol* 2008;28:665–671.
43. Manoli M, Driever W. Fluorescence-activated cell sorting (FACS) of fluorescently tagged cells from zebrafish larvae for RNA isolation. *Cold Spring Harb Protoc* 2012;2012: pdb.prot069633.
44. Nick JA, Young SK, Brown KK, et al. Role of p38 mitogen-activated protein kinase in a murine model of pulmonary inflammation. *J Immunol* 2000;164:2151–2159.

Received February 25, 2023. Accepted June 27, 2023.

Correspondence

Address correspondence to: Junping Shi, MD, PhD, Department of Infectious Disease, Institute of Translational Medicine, Institute of Hepatology and Metabolic Diseases, The Affiliated Hospital of Hangzhou Normal University, No. 126 Wenzhou Road, Hangzhou, Zhejiang 310015, China. e-mail: 20131004@hznu.edu.cn.

CRedit Authorship Contributions

Junping Shi (Conceptualization: Lead; Supervision: Lead; Writing – review & editing: Lead)

Xiaoxiao Mi (Data curation: Lead; Formal analysis: Lead; Funding acquisition: Lead; Investigation: Lead; Methodology: Lead; Software: Lead; Validation: Lead; Visualization: Lead; Writing – original draft: Lead)

Yu Song (Data curation: Supporting; Software: Lead)

Chaohua Deng (Methodology: Supporting; Validation: Lead)

Jian Yan (Methodology: Lead; Validation: Lead; Visualization: Lead)

Zhihui Li (Data curation: Equal; Methodology: Equal)

Yingniang Li (Investigation: Supporting; Methodology: Supporting; Validation: Supporting)

Jun Zheng (Methodology: Equal; Visualization: Equal)

Wenjun Yang (Investigation: Supporting; Validation: Supporting)

Ling Gong (Investigation: Supporting; Methodology: Supporting)

Conflicts of interest

The authors disclose no conflicts.

Funding

This research was supported by the National Natural Science Foundation of China grant 82100614 and the Joint Funds of the Zhejiang Provincial Natural Science Foundation of China grant LBY21H030001.

Data Availability Statement

The raw RNA sequencing data can be provided upon reasonable request.